Computational Thermal Sciences, 4 (1): 77–97 (2012)

BOUNDARY CONDITION EFFECTS ON NATURAL CONVECTION OF BINGHAM FLUIDS IN A SQUARE ENCLOSURE WITH DIFFERENTIALLY HEATED HORIZONTAL WALLS

Osman Turan,[1] Robert J. Poole,[2] & Nilanjan Chakraborty[3,*]

[1]*Deptartment of Mechanical Engineering, Karadeniz Technical University, Turkey*

[2]*School of Engineering, University of Liverpool, United Kingdom*

[3]*School of Mechanical and Systems Engineering, Newcastle University, United Kingdom*

[*]Address all correspondence to Nilanjan Chakraborty
E-mail: nilanjan.chakraborty@newcastle.ac.uk

Natural convection of Bingham fluids in square enclosures with differentially heated horizontal walls has been numerically analyzed for both constant wall temperature (CWT) and constant wall heat flux (CWHF) boundary conditions for different values of Bingham number Bn (i.e., nondimensional yield stress) for nominal Rayleigh and Prandtl numbers ranging from 10^3 to 10^5 and from 0.1 to 100, respectively. A semi-implicit pressure-based algorithm is used to solve the steady-state governing equations in the context of the finite-volume methodology in two dimensions. It has been found that the mean Nusselt number $\overline{Nu}$ increases with increasing Rayleigh number, but $\overline{Nu}$ is found to be smaller in Bingham fluids than in Newtonian fluids (for the same nominal values of Rayleigh and Prandtl numbers) due to augmented flow resistance in Bingham fluids. Moreover, $\overline{Nu}$ monotonically decreases with increasing Bingham number irrespective of the boundary condition. Bingham fluids exhibit nonmonotonic Prandtl number Pr dependence on $\overline{Nu}$ and a detailed physical explanation has been provided for this behavior. Although variation of $\overline{Nu}$ in response to changes in Rayleigh, Prandtl, and Bingham numbers remains qualitatively similar for both CWT and CWHF boundary conditions, $\overline{Nu}$ for the CWHF boundary condition for high values of Rayleigh number is found to be smaller than the value obtained for the corresponding CWT configuration for a given set of values of Prandtl and Bingham numbers. The physical reasons for the weaker convective effects in the CWHF boundary condition than in the CWT boundary condition, especially for high values of Rayleigh number, have been explained through a detailed scaling analysis. The scaling relations are used to propose correlations for $\overline{Nu}$ for both CWT and CWHF boundary conditions and the correlations are shown to capture $\overline{Nu}$ satisfactorily for the range of Rayleigh, Prandtl, and Bingham numbers considered in this analysis.

KEY WORDS: *natural convection, Bingham fluid, yield stress, Rayleigh number, Prandtl number, Nusselt number, boundary conditions*

1. INTRODUCTION

Natural convection in rectangular enclosures is one of the most extensively analyzed configurations in the heat transfer literature [e.g., de Vahl Davis (1983); Ostrach (1988)]. This configuration is of fundamental importance because of its application in electronic cooling, meteorology, solar collectors, and food preservation and heating. Several possible configurations are possible for natural convection within rectangular enclosures based on different boundary conditions. One of the most important variants of natural convection in rectangular enclosures is the configuration where the horizontal walls are differentially heated through the bottom wall and the vertical walls are kept adiabatic. This configuration is commonly referred to as the Rayleigh–Bénard (RB) configuration and the present study will mainly focus on this configuration for both constant wall temperature (CWT) and constant wall

1940–2503/12/$35.00

heat flux (CWHF) boundary conditions for the differentially heated horizontal walls.

To date, most analyses on natural convection in rectangular enclosures have been carried out for Newtonian fluids, and an extensive review is contained in Ostrach (1988). In comparison, relatively little effort was devoted to natural convection of non-Newtonain fluids [e.g., Ozoe and Churchill (1972)]. Yield stress fluid is a special type of non-Newtonian fluid which behaves like a fluid only when a threshold stress (i.e., yield stress) is surpassed (Barnes, 1999) and behaves like a solid below the yield stress. Bingham fluid is a special type of yield stress fluid, which exhibits a linear relation between shear stress and the rate of shear once the yield stress is surpassed (Barnes, 1999). There have been some analyses of RB configuration involving non-Newtonian fluids [e.g., Park and Ryu (2001); Lamsaadi et al. (2005); Zhang et al. (2006); Balmforth and Rust (2009)]. However, the aforementioned studies mainly concentrated on the critical condition under which the fluid flow initiates within the enclosure. However, the heat transfer within the enclosure remains purely conduction driven in the absence of fluid flow within the enclosure and the fluid flow under critical condition is unlikely to be strong enough to significantly influence the overall heat transfer within the enclosure. This is reflected in the unity value of mean Nusselt number $\overline{\mathrm{Nu}}$ under critical and subcritical conditions. The present study concentrates on the conditions under which fluid flow remains strong enough to influence the heat transfer rate significantly and the mean Nusselt number $\overline{\mathrm{Nu}}$ remains greater than unity (i.e., $\overline{\mathrm{Nu}} > 1.0$). The influences of boundary conditions on natural convection of Bingham fluids in square enclosures with differentially heated horizontal walls are yet to be analyzed in the literature. This paper aims to address the aforementioned gap in the literature by carrying out numerical simulations as done previously by the present authors for square enclosures subjected to differentially heated vertical side walls (Turan et al., 2010, 2011). The physics of natural convection in enclosures with differentially heated horizontal walls is fundamentally different from natural convection in enclosures with differentially heated vertical side walls [which was analyzed earlier by Turan et al. (2010, 2011)] and this will be discussed in a more detailed manner in the Results and Discussion section of this paper. In this respect, the main objectives of this analysis are as follows:

1. To analyze natural convection of Bingham fluids in RB configurations for both CWT and CWHF boundary conditions using numerical simulations.
2. To explain the differences in heat transfer rate of Bingham fluids for both CWT and CWHF boundary conditions in the RB configuration.
3. To propose correlations for $\overline{\mathrm{Nu}}$ for natural convection of Bingham fluids in square enclosures for both CWT and CWHF boundary conditions as a function of nominal Rayleigh, Bingham, and Prandtl numbers.

To meet the above objectives, numerical simulations of natural convection of Bingham fluids in square RB configuration have been carried out for nominal Rayleigh and Prandtl numbers ranging from 10^3 to 10^5 and from 0.1 to 100, respectively, for both the CWT and CWHF boundary conditions. The biviscosity regularization as proposed by O'Donovan and Tanner (1984) is used for the simulations, which effectively replaces the unyielded solidlike region by a region of very high viscosity. The accuracy of the biviscosity assumption has been assessed by carrying out some representative simulations using an alternative exponential function-based regularization by Papanastasiou (1987) and the agreement has been found to be excellent in all cases (e.g., maximum difference in $\overline{\mathrm{Nu}}$ remains of the order of 2%).

The rest of the paper will be organized as follows. The necessary mathematical background relevant to this analysis will be provided in the next section. This will be followed by a brief description on the numerical implementation. Following this, results will be presented and subsequently discussed. Finally the main findings will be summarized and conclusions will be drawn.

2. MATHEMATICAL BACKGROUND

The Bingham model for yield stress fluids can be expressed in the following manner (Barnes, 1999):

$$\underline{\underline{\dot{\gamma}}}=0 \ \text{ for } \ \tau \le \tau_y, \ \ \underline{\underline{\tau}}=(\mu+\tau_y/\dot{\gamma})\underline{\underline{\dot{\gamma}}} \ \text{ for } \ \tau > \tau_y \quad (1)$$

where $\dot{\gamma} = (\partial u_i/\partial x_j + \partial u_j/\partial x_i)$ are the components of the rate of strain tensor $\underline{\underline{\dot{\gamma}}}$, $\underline{\underline{\tau}}$ is the stress tensor, τ_y is the yield stress, μ is the so-called plastic viscosity of the yielded fluid, and τ and $\dot{\gamma}$ are the second invariants of the stress and the rate of strain tensors in a pure shear flow, respectively, which are expressed as

$$\tau = [\underline{\underline{\tau}} : \underline{\underline{\tau}}/2]^{1/2}; \quad \dot{\gamma} = [\underline{\underline{\dot{\gamma}}} : \underline{\underline{\dot{\gamma}}}/2]^{1/2} \quad (2)$$

O'Donovan and Tanner (1984) proposed the biviscosity model to mimic the stress-shear rate characteristics for a Bingham fluid as

$$\underline{\underline{\tau}} = \mu_{\text{yield}} \underline{\underline{\dot{\gamma}}} \quad \text{for} \quad \dot{\gamma} \leq \tau_y/\mu;$$
$$\underline{\underline{\tau}} = \underline{\underline{\tau_y}} + \mu[\underline{\underline{\dot{\gamma}}} - \underline{\underline{\tau_y}}/\mu_{\text{yield}}] \quad \text{for} \quad \dot{\gamma} > \tau_y/\mu_{\text{yield}} \tag{3}$$

where $\underline{\underline{\tau_y}}$ is the yield stress tensor, μ_{yield} is the yield viscosity, and μ is the plastic viscosity. This model replaces the solid material by a fluid of high viscosity and it was suggested by O'Donovan and Tanner (1984) that a value of μ_{yield} equal to 1000μ mimics the true Bingham model in a satisfactory manner. In the present study the biviscosity model is predominantly used but in order to assess the sensitivity of the simulations on the choice of regularization, a limited number of simulations have also been carried out based on the regularization proposed by Papanastasiou (1987):

$$\underline{\underline{\tau}} = \underline{\underline{\tau_y}} [1 - \exp(-m\dot{\gamma})] + \mu \underline{\underline{\dot{\gamma}}} \tag{4}$$

where *m* is the stress growth exponent which has the dimensions of time. The regularization given by Eq. (4) also transforms the "unyielded" region to a zone of high viscosity. The maximum difference between the mean Nusselt number obtained from the biviscosity and Papanastasiou regularizations remains of the same order as the typical experimental and numerical uncertainties (∼2%–3%).

It is worth noting that biviscosity and exponential regularizations by O'Donovan and Tanner (1984) and Papanastasiou (1987) respectively approximate the strain rate dependences of shear stress for Bingham fluids and the unyielded zone is modeled by zones of high viscosity in both regularizations, albeit in two different manners. In the bi-viscosity regularization the relation between shear stress and strain rate is discontinuous [see Eq. (3)]. In contrast, the strain rate dependence of shear stress is continuous according to the regularization proposed by Papanastasiou (1987) [see Eq. (4)]. Both regularizations give the same expression of stress tensor (i.e., $\underline{\underline{\tau}} = \underline{\underline{\tau_y}} + \mu \underline{\underline{\dot{\gamma}}}$) for the fully yielded region. It is true that the choice of μ_{yield} may have some impact on the results in the biviscosity regularization but it was suggested by O'Donovan and Tanner (1984) that a value of $\mu_{\text{yield}} \geq 10^3\mu$ mimics the true Bingham model in a satisfactory manner. A sensitivity analysis has been carried out to assess the sensitivity of the simulations on the choice of μ_{yield}. It has been found that the maximum difference in mean Nusselt number remains about 0.5% when μ_{yield} is altered from $10^3\mu$ to $10^4\mu$.

Using Buckingham's pi theorem it is possible to show that the Nusselt number $\text{Nu} = hL/k$ for a square enclosure of dimension L can be expressed as: $\text{Nu} = f_1$ ($\text{Ra}_{CWT}, \text{Bn}_{CWT}, \text{Pr}$) ($\text{Nu} = f_2$ ($\text{Ra}_{CWHF}, \text{Bn}_{CWHF}$, Pr)) for the CWT (CWHF) boundary condition, where the nominal Rayleigh, Bingham, and Prandtl numbers are given by (Turan et al., 2010, 2011)

$$\text{Ra}_{CWT} = \rho g \beta (T_H - T_C) L^3/\mu\alpha = \text{Gr}_{CWT}\text{Pr};$$
$$\text{Ra}_{CWHF} = \rho g \beta q L^4/k\mu\alpha = \text{Gr}_{CWHF}\text{Pr} \tag{5a}$$

$$\text{Bn}_{CWT} = \tau_y L/\mu\sqrt{g\beta(T_H - T_C)L};$$
$$\text{Bn}_{CWHF} = \tau_y/\mu\sqrt{g\beta q/k}, \quad \text{and} \quad \text{Pr} = \mu c_p/k \tag{5b}$$

where $\text{Gr}_{CWT} = \rho^2 g\beta(T_H - T_C)L^3/\mu^2$ ($\text{Gr}_{CWHF} = \rho^2 g\beta q L^4/k\mu^2$) is the Grashof number in the CWT (CWHF) configuration, T_H and T_C are the hot and cold wall temperatures in the CWT configuration, q is the wall heat flux, c_p is the specific heat, and k is the thermal conductivity. The local heat transfer coefficient h is defined as

$$h = |-k(\partial T/\partial y)_{wf} \times 1/(T_{\text{wall}} - T_{\text{ref}})| \tag{6}$$

where the subscript "*wf*" refers to the condition of the fluid in contact with the wall, T_{wall} is the wall temperature, and T_{ref} is the appropriate reference temperature, which can be taken to be the cold wall(hot wall) temperature for the hot (cold) wall, respectively. The Bingham number represents the ratio of yield stress to viscous stresses. In Bingham fluid flows the viscosity varies throughout the flow and an effective viscosity expressed as $\mu_{\text{eff}} = \tau_y/\dot{\gamma} + \mu$ might be more representative of the viscous stress within the flow than the constant plastic viscosity μ.Therefore the Rayleigh, Prandtl, and Bingham numbers could have been defined more appropriately if μ_{eff} was used instead of μ. However, $\dot{\gamma}$ is expected to show local variations in the flow domain so using a single characteristic value in the definitions of the nondimensional numbers may not yield any additional benefit in comparison to the definitions given by Eqs. (5a) and (6). In the present study the effects of Rayleigh, Bingham, and Prandtl numbers on the Nusselt number are investigated systematically and suitable correlations proposed. However, it is worth noting that in the present study the plastic viscosity $\mu$and yield stress τ_y are taken to be independent of temperature for the sake of simplicity and also due to the experimental evidence that the yield stress remains approximately independent of temperature and the plastic viscosity is only a weakly decreasing function of temperature for a well-known yield stress model system ("Carbopol") in the temperature range 0°C–90°C (Peixinho et

al., 2008). However, such temperature dependence will be substance dependent although the data available are very scant. Given this paucity of data, this analysis is aimed at fundamental understanding of the influences of CWT and CWHF boundary conditions on natural convection of Bingham fluids in square enclosures with differentially heated horizontal walls, and as a first attempt the temperature dependences of thermophysical properties (e.g., k, c_p, μ, and τ_y) are not accounted for in the current analysis. Similar assumptions have been made in several previous studies on natural convection involving both Newtonian and Bingham fluids (de Vahl Davis, 1983; Bejan, 1984; Ostrach, 1988; Zhang et al., 2006; Vola et al., 2003; Vikhansky, 2009; 2010; Turan et al., 2010, 2011). Moreover, temperature dependence of thermophysical quantities does not change the essential physics of the problem so the convection pattern is unlikely to be altered by the temperature dependence of thermophysical properties.

3. NUMERICAL IMPLEMENTATION

For the present study steady-state flow of an incompressible Bingham fluid is considered. The governing equations for incompressible fluids under steady state take the following form:

$$\text{Mass conservation equation: } \partial u_i/\partial x_i = 0 \tag{7a}$$

$$\text{Momentum transport equations: } \rho u_j(\partial u_i/\partial x_j) = -\partial P/\partial x_i + \rho g \beta \delta_{i2}(T - T^*) + \partial \tau_{ij}/\partial x_j \tag{7b}$$

$$\text{Energy conservation equation: } \rho c_p u_j(\partial T/\partial x_j) = k(\partial^2 T/\partial x_j \partial x_j) \tag{7c}$$

where T^* is the reference temperature for evaluating the buoyancy term $\rho g \delta_{i2} \beta (T–T^*)$ in the momentum transport equations which is taken to be the cold wall temperature T_C and the temperature at the center of the domain T_{cen} for CWT and CWHF boundary conditions, respectively. The stress tensor is evaluated using either Eq. (3) (bi-viscosity approach) or Eq. (4) (Papanastasiou regularization). The viscous dissipation effects are neglected in the current analysis following several previous studies on natural convection of both Newtonian and Bingham fluids (de Vahl Davis, 1983; Bejan, 1984; Ostrach, 1988; Zhang et al., 2006; Vola et al., 2003; Vikhansky, 2009, 2010; Turan et al., 2010, 2011). The viscous dissipation effects are expected to play a key role in natural convection under the condition where kinetic energy of the fluid becomes of the same order as thermal energy (Gebhart, 1962), which can be realized when $g\beta L_{\text{ref}}/c_p \gg 1$ where L_{ref} is an appropriate length scale. However, Gebhart (1962) demonstrated that $g\beta/c_p$ remains extremely small for most common fluids ($\sim 10^{-9}$–10^{-6} m^{-1}) and thus requires an extremely large length scale L_{ref} for which viscous dissipation starts to affect heat and momentum transport (Gebhart, 1962). As this analysis does not attempt to address extremely large scale applications, the effects of viscous dissipation could be neglected here without much loss of generality following previous studies (de Vahl Davis, 1983; Bejan, 1984; Ostrach, 1988; Zhang et al., 2006; Vola et al., 2003; Vikhansky, 2009, 2010; Turan et al., 2010, 2011).

In the biviscosity approximation to the Bingham model, the ratio of the yield viscosity (μ_{yield}) to the plastic viscosity (μ) was taken to be 10^4. In order to assess the sensitivity of the value of μ_{yield}, the simulations have been carried out for both $\mu_{\text{yield}} = 10^3\mu$ and $\mu_{\text{yield}} = 10^4\mu$, and the quantitative agreement between the results are found to be satisfactory for all cases (i.e., maximum deviation in $\overline{\text{Nu}} = \int_0^L \text{Nu}\, dx_1/L$ is of the order of 0.5%). Given this agreement, only the results corresponding to $\mu_{\text{yield}} = 10^4\mu$ are presented in this paper as a greater magnitude of μ_{yield} provides a more accurate description of Bingham fluid flow in the context of biviscosity regularization.

A finite-volume code is used to solve the coupled governing equations. In this framework, a second-order central differencing is used for the diffusive terms and a second-order up-wind scheme is used for the convective terms. Coupling of the pressure and velocity is achieved using the well-known SIMPLE (semi-implicit method for pressure-linked equations) algorithm (Patankar, 1980). The convergence criteria were set to 10^{-9} for all the relative (scaled) residuals.

The simulation domain is shown schematically in Fig. 1 where the two horizontal walls of a square enclosure are kept at different temperatures with the lower wall kept at higher temperature ($T_H > T_C$). The vertical walls are considered to be adiabatic in nature. Both velocity components (i.e., u_1 and u_2) are identically zero on each boundary because of the no-slip condition and impenetrability of rigid boundaries. The temperatures for cold and hot horizontal walls are specified (i.e., $T(x_2 = 0) = T_H$ and $T(x_2 = L) = T_C$). The temperature boundary conditions for the vertical insulated boundaries are given by $\partial T/\partial x_1 = 0$ at $x_1 = 0$ and $x_1 = L$.

The grid independence of the results has been established based on a careful analysis of four different nonuni-

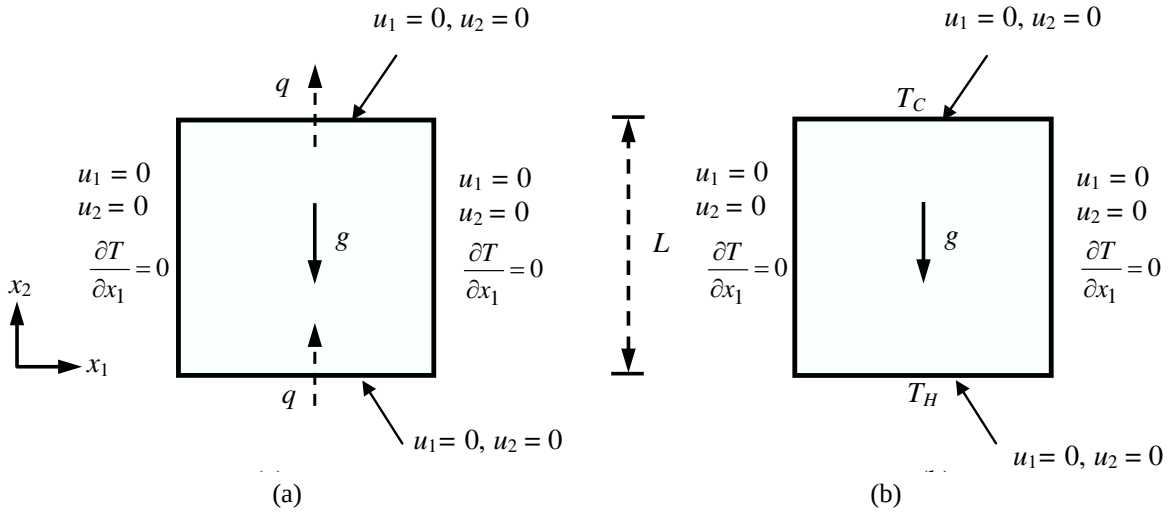

FIG. 1: Schematic diagram of the simulation domain: **(a)** constant wall heat flux and **(b)** constant wall temperature.

form meshes M1 (20×20), M2 (40×40), M3 (80×80), and M4 (160×160), and their details are provided in Table 1. For some representative simulations [Newtonian ($\mathrm{Bn}_{CWT} = 0$ and $\mathrm{Bn}_{CWHF} = 0$) and $\mathrm{Bn}_{CWT} = \mathrm{Bn}_{CWHF} = 0.25$ for $\mathrm{Ra}_{CWT} = \mathrm{Ra}_{CWHF} = 10^5$ and Pr = 10] the numerical uncertainty is quantified here using Richardson's extrapolation theory (Roache, 1997). For a primitive variable ϕ the Richardson's extrapolation value is given by $\phi_{h=0} = \phi_1 + (\phi_2 - \phi_1)/(r^p - 1)$, where ϕ_1 is obtained based on fine grid and ϕ_2 is the solution based on next level of coarse grid, r is the ratio between coarse to fine grid spacings, and p is the theoretical order of accuracy. In this analysis the apparent order p was taken to be 2 as a second-order central differencing is used for the diffusive terms and a second-order up-wind scheme is used for the convective terms. The numerical uncertainties for the mean Nusselt number $\overline{\mathrm{Nu}}$ and the maximum nondimensional horizontal velocity ($U_{\max}$) magnitude on the vertical midplane of the enclosure are presented in Table 2. As seen in Table 2, the maximum numerical uncertainty between meshes remains at most 4.7 % for $U_{\max}$ in all cases. The uncertainty in $\overline{\mathrm{Nu}}$ is considerably smaller than this value (< 0.25%). Based on these uncertainties the simulations were conducted on mesh M3 which provided a reasonable computational efficiency.

The yield stress simulations have been conducted for Bingham numbers Bn ranging from 0 to $\mathrm{Bn}_{\max}$ where $\mathrm{Bn}_{\max}$ is the Bingham number at which the mean Nusselt number $\overline{\mathrm{Nu}}$ approaches unity (i.e., $\overline{\mathrm{Nu}} = 1.0$) and the solution essentially becomes the steady-state pure-conduction result.

4. RESULTS AND DISCUSSION

4.1 Effects of Rayleigh Number

The variations of nondimensional temperature for both CWT and CWHF boundary conditions (i.e., $\theta_{CWT} = (T - T_{\mathrm{cen}})/(T_H - T_C)$ and $\theta_{CWHF} = (T - T_{\mathrm{cen}})k/qL$) and nondimensional horizontal velocity component $U = u_1 L/\alpha$ along the vertical midplane are shown in Fig. 2 for both Newtonian and a representative Bingham fluid case (i.e., $\mathrm{Bn}_{CWT} = \mathrm{Bn}_{CWHF}$ = 0.25). The variations of the vertical velocity component are not explicitly shown because the magnitudes of u_1 and u_2 remain of the same

TABLE 1: Nondimensional minimum cell distance ($\Delta_{\min,\mathrm{cell}}/L$) and grid expansion ratio (r) values

Grid	M1 20×20	M2 40×40	M3 80×80	M4 160×160
$(\Delta_{\min,\mathrm{cell}}/L)$	4.1325×10^{-3}	1.8534×10^{-3}	8.7848×10^{-4}	4.3001×10^{-4}
r	1.5137	1.2303	1.1092	1.0532

TABLE 2: Numerical uncertainty for mean Nusselt number and maximum nondimensional horizontal velocity component on the vertical midplane for CWHF boundary condition at $\mathrm{Ra}_{CWHF} = 1\times10^5$ and Pr = 10 for Newtonian and Bingham ($\mathrm{Bn}_{CWHF} = 0.25$) fluids

		$\overline{\mathbf{Nu}}$			$U_{\max}$		
		M2	**M3**	**M4**	**M2**	**M3**	**M4**
Newtonian fluid	ϕ	3.3742	3.3795	3.3816	42.9983	43.4817	43.6733
	ϕ_{ext}	3.3823			43.7370		
	e_{ext} (%)	0.2395	0.0828	0.0207	1.6893	0.5841	0.1460
Bingham fluid (Bn = 0.25)	ϕ	3.0236	3.0255	3.0276	28.5689	29.5763	29.8815
	ϕ_{ext}	3.0283			29.9830		
	e_{ext} (%)	0.1552	0.0924	0.0231	4.7171	1.3572	0.3393

order in square enclosures as governed by the continuity relation (i.e., $u_1/L \sim u_2/L$). It is evident from Fig. 2 that the magnitude of U and the nonlinearity of the temperature variation with the vertical direction increase with increasing Rayleigh number for both CWT and CWHF boundary conditions. Equating order of magnitudes of inertial and buoyancy terms of the momentum equation yields $\vartheta^2/L \sim g\beta\Delta T$ where ϑ is a characteristic velocity scale and ΔT is the temperature difference between the horizontal walls, which is taken to scale with $q\delta_{th}/k$ for the CWHF boundary condition as wall heat flux q scales as $q \sim k\Delta T/\delta_{th}$. In the case of the CWT boundary condition ΔT remains exactly equal to $(T_H - T_C)$. This suggests that U scales in the following manner for the CWT and CWHF boundary conditions:

$$U \sim \vartheta L/\alpha \sim \sqrt{g\beta\Delta T L\times}L/\alpha \sim \sqrt{\mathrm{Ra}_{CWT}\mathrm{Pr}} \quad \text{(for CWT)} \tag{8a}$$

$$U \sim \vartheta L/\alpha \sim \sqrt{g\beta q\delta_{th}L/k\times}L/\alpha \sim \sqrt{\mathrm{Ra}_{CWHF}\mathrm{Pr}(\delta_{th}/L)} \quad \text{(for CWHF)} \tag{8b}$$

Equations (8a) and (8b) indicate that U is expected to increase with increasing Rayleigh number for both Newtonian and Bingham fluids which is consistent with the observations from Fig. 2. Moreover, it can be seen from Eqs. (8a) and (8b) that U is expected to assume a smaller value in the case of the CWHF boundary condition than in the CWT boundary condition for the same numerical values of Ra_{CWT} and Ra_{CWHF} as $\delta_{th} \ll L$ for the regime of convection where boundary-layer transport plays a key role. The aforementioned difference in the behavior of U between the CWT and CWHF boundary conditions for a given set of values of Rayleigh and Prandtl numbers can also be substantiated from Fig. 2 which shows that U assumes a smaller magnitude in the CWHF case than in the CWT case for the same numerical values of Rayleigh number for both Newtonian and Bingham fluids. However, the flow resistance in Bingham fluids is greater than Newtonian fluids and this is reflected in the smaller magnitude of U in the Bingham fluid than in the Newtonian fluid for the same nominal value of Rayleigh number, which can also be confirmed from Fig. 2. The magnitude of U represents the strength of advection within the enclosure and thus the variation of nondimensional temperature becomes increasingly nonlinear with increasing Rayleigh number for both Newtonian and Bingham fluids. The pure-conduction solution yields a linear variation of nondimensional temperature between the horizontal walls and the extent of the nonlinearity of temperature distribution in the vertical direction depends on the strength of thermal advection. The strong thermal gradients are confined to the thermal boundary layers adjacent to the walls under the conditions in which advective transport plays a key role.

For small values of Rayleigh number the heat transfer within the enclosure takes place purely due to thermal conduction and under that condition the temperature difference between the horizontal walls for the CWHF boundary condition becomes $\Delta T_{\mathrm{cond}} = qL/k$ and this becomes exactly equal to $(T_H - T_C)$ for the CWT boundary condition with the same numerical values of Rayleigh number as the definitions of Ra_{CWT} and Ra_{CWHF} are equivalent to each other under the pure conduction-driven heat transfer. The temperature difference between the horizontal walls ΔT scales as $\Delta T \sim q\delta_{th}/k \sim qL/k(\delta_{th}/L)$ which suggests that the magnitude of θ_{CWHF} scales as $\theta_{CWHF} \sim \Delta T k/qL \sim \delta_{th}/L$ whereas the magnitude of θ_{CWT} remains of the order of

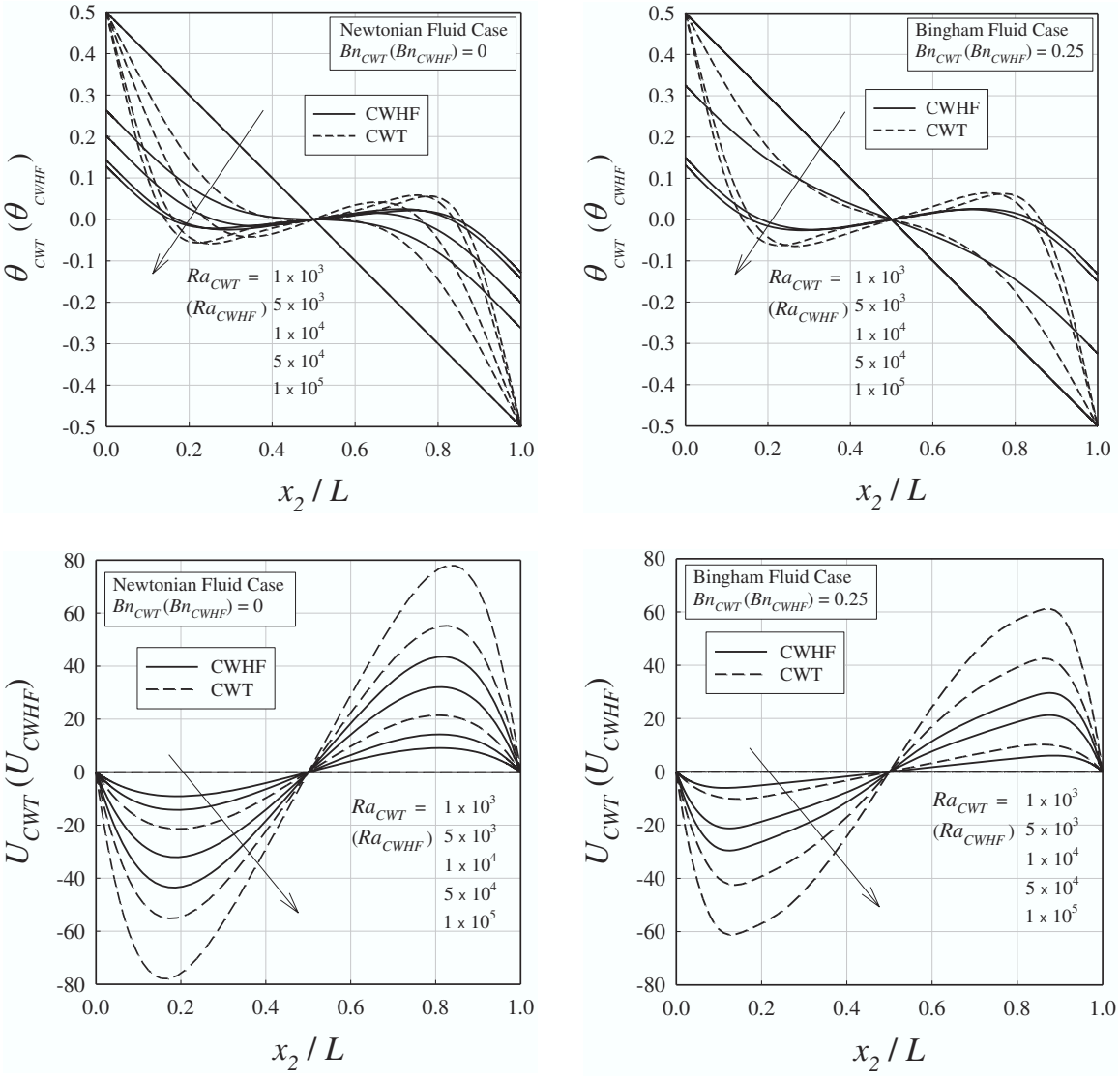

(a) (b)

FIG. 2: Variations of nondimensional temperature θ_{CWT} (θ_{CWHF}) and horizontal velocity component $U_{CWT}(U_{CWHF})$ along the vertical midplane (i.e., along x_1/L = 0.5) for different values of Rayleigh number Ra_{CWT} (Ra_{CWHF}) at Pr = 10: **(a)** Newtonian fluid, **(b)** Bingham fluid ($\mathrm{Bn}_{CWT} = \mathrm{Bn}_{CWHF}$ = 0.25).

unity (i.e., the maximum magnitude of θ_{CWT} is equal to 0.5) as the temperature difference between the horizontal walls remains unchanged in the case of the CWT boundary condition. It can be seen from Fig. 2 that the maximum value of θ_{CWHF} remains smaller than that of θ_{CWT} for the same numerical value of nominal Rayleigh number under the conditions in which thermal advection has a significant influence on thermal transport within the enclosure. The smaller values of ΔT in the CWHF case induce a weaker buoyancy force than that in the CWT case, which is reflected in the smaller magnitude of U in the CWHF boundary condition than in the CWT boundary condition.

Figure 2 shows that the magnitude of the thermal gradient $\partial T/\partial x_2$ in the case of the CWT boundary condition increases with increasing Ra_{CWT} for both Newtonian and Bingham fluids as the thermal boundary-layer thickness decreases with strengthening of advective transport. The

behavior of the thermal boundary-layer thickness in relation to the nominal Rayleigh number can be illustrated by equating the order of magnitudes of the inertial and viscous terms of the momentum conservation equation in the vertical direction (Turan et al., 2010, 2011):

$$\rho\vartheta^2/L \sim (\tau_y + \mu\vartheta/\delta)/\delta \tag{9}$$

where δ is the hydrodynamic boundary-layer thickness. Equation (9) yields the following scaling of δ for the CWT boundary condition (Turan et al., 2010, 2011):

$$\delta \sim 0.5(\tau_y L/\rho\vartheta^2) + 0.5(L/\rho\vartheta^2)\sqrt{\tau_y^2 + 4\rho\vartheta^3\mu/L} \tag{10}$$

Using $\vartheta \sim \sqrt{g\beta(T_H - T_C)L}$ in Eq. (10) yields the following estimation of δ:

$$\delta \sim \frac{\mu/\rho}{\sqrt{g\beta\Delta T L}}\left[\frac{\mathrm{Bn}_{CWT}}{2} + \frac{1}{2} \times \sqrt{\mathrm{Bn}_{CWT}^2 + 4\left(\frac{\mathrm{Ra}_{CWT}}{\mathrm{Pr}}\right)^{1/2}}\right] \tag{11}$$

Thus, the thermal boundary-layer thickness δ_{th} for CWT boundary condition scales in the following manner:

$$\delta_{th} \sim \min\left[L, \frac{L\mathrm{Pr}^{1/2}}{\mathrm{f}_3(\mathrm{Ra}_{CWT}, \mathrm{Bn}, \mathrm{Pr})\mathrm{Ra}_{CWT}^{1/2}} \times \left[\frac{\mathrm{Bn}_{CWT}}{2} + \frac{1}{2}\sqrt{\mathrm{Bn}_{CWT}^2 + 4\left(\frac{\mathrm{Ra}_{CWT}}{\mathrm{Pr}}\right)^{1/2}}\right]\right] \tag{12}$$

where the thermal boundary-layer thickness δ_{th} is related to the hydrodynamic boundary-layer thickness δ in the following manner: $\delta/\delta_{th} = f_3(\mathrm{Ra}_{CWT}, \mathrm{Bn}_{CWT}, \mathrm{Pr})$ with $f_3(\mathrm{Ra}_{CWT}, \mathrm{Bn}_{CWT}, \mathrm{Pr})$ as a function of Rayleigh, Prandtl, and Bingham numbers, which is expected to increase with increasing Prandtl number. According to Eq. (12) δ_{th} is expected to decrease with increasing Ra_{CWT} in the case of both Newtonian and Bingham fluids, as observed in Fig. 2. Equation (12) further indicates that δ_{th} for Bingham fluid is likely to be thicker than that in the case of Newtonian fluids for the same nominal values of Ra_{CWT} and Pr, which can also be confirmed from the θ_{CWT} distribution with x_2/L (see Fig. 2). Using $\vartheta \sim \sqrt{g\beta q\delta_{th}L/k}$ in Eq. (9) yields the following expression for the CWHF boundary condition (Turan et al., 2011):

$$\sqrt{\frac{\mathrm{Ra}_{CWHF}}{\mathrm{Pr}}}\left(\frac{\delta_{th}}{L}\right)^{5/2} \sim \frac{\mathrm{Bn}_{CWHF}\,(\delta_{th}/L)^{1/2}}{f_4\,(\mathrm{Ra}_{CWHF}, \mathrm{Pr}, \mathrm{Bn}_{CWHF})} + \frac{1}{f_4^2\,(\mathrm{Ra}_{CWHF}, \mathrm{Pr}, \mathrm{Bn}_{CWHF})} \tag{13}$$

where $\delta/\delta_{th} = f_4(\mathrm{Ra}_{CWHF}, \mathrm{Bn}_{CWHF}, \mathrm{Pr})$ with $f_4(\mathrm{Ra}_{CWHF}, \mathrm{Bn}_{CWHF}, \mathrm{Pr})$ being a function of Rayleigh, Prandtl, and Bingham numbers, which is expected to increase with increasing Prandtl number in the case of the CWHF boundary condition. Equation (13) is not solvable analytically but this equation can be used to obtain qualitative information regarding the expected behaviors. Under the condition $\mathrm{Bn}_{CWHF}(\delta_{th}/L)^{1/2}/f_4 \ll 1/f_4^2$, one obtains $\delta_{th} \sim L(\mathrm{Pr}/\mathrm{Ra}_{CWHF})^{1/5} f_4^{-0.8}$ whereas the condition given by $\mathrm{Bn}_{CWHF}(\delta_{th}/L)^{1/2}/f_4 \gg 1/f_4^2$ leads to $\delta_{th} \sim L(\mathrm{Pr}/\mathrm{Ra}_{CWHF})^{1/4}\mathrm{Bn}_{CWHF}^{1/2} f_4^{-0.5}$. These relations suggest that δ_{th} is expected to decrease with increasing Ra_{CWHF}, whereas δ_{th} is expected to increase with increasing Bn_{CWHF} for a given value of nominal value of Ra_{CWHF} also in the case of the CWHF boundary condition. The decrease (increase) in δ_{th} with increasing Ra_{CWHF} (Bn_{CWHF}) gives rise to a decrease (an increase) in the magnitude of $\theta_{CWHF} \sim \delta_{th}/L$ with rising Rayleigh (Bingham) number in the CWHF boundary condition, which can also be confirmed from inspection of Fig. 2.

The contours of nondimensional temperature θ_{CWHF} and stream function $\Psi = \psi/\alpha$ (with ψ being the dimensional stream function) for Bn_{CWHF} = 0 (i.e., Newtonian) and Bn_{CWHF} = 0.25 for different values of Ra_{CWHF} are shown in Fig. 3. The corresponding variations for the CWT boundary condition are not explicitly shown here because of their qualitative similarities to the CWHF variations. It is evident from Fig. 3 that the isotherms remain parallel to the horizontal boundaries for small value of Ra_{CWHF} where the heat transfer is primarily conduction driven. As the circulation patterns remain qualitatively similar at a given Rayleigh number, the isotherms for both Bn_{CWHF} = 0 (i.e., Newtonian) and Bn_{CWHF} = 0.25 cases look similar. The "unyielded" zones according to the criterion proposed by Mitsoulis (2007) (i.e., zones of fluid where $\sqrt{\tau_{12}\tau_{12}} \leq \tau_y$) are also shown in gray shading in Fig. 3 for Bn = 0.25. It is worth noting that these zones are not truly "unyielded" as indicated by Mitsoulis and Zisis (2001). In the results shown in Fig. 3 a biviscosity regularization is employed to account for the Bingham fluid flow so there will always be extremely slowly moving fluid flow within these essentially very high viscosity regions, which Mitsoulis and

Zisis (2001) termed as the "apparently unyielded regions (AUR)," It is important to indicate that the small islands of AUR alter with increasing values of μ_{yield} (shown in Fig. 3 for $\mu_{\text{yield}} = 10^4\mu$) while the mean Nusselt number and the stream function are independent of μ_{yield} for $\mu_{\text{yield}} \geq 10^3\mu$, which is consistent with earlier findings by Beverly and Tanner (1989) for a different flow configuration. For a given value of τ_y the AURs, which satisfy $\sqrt{\tau_{12}\tau_{12}} \leq \tau_y$, are expected to shrink with an increase in μ_{yield}. As the AURs are dependent on the precise choice of μ_{yield} and the value of $\overline{\text{Nu}}$ remains independent of the shape and size of AURs for $\mu_{\text{yield}} \geq 10^3\mu$, their effects on heat transfer are not important and thus will not be discussed in this paper. As $\mu_{\text{yield}} = 10^4\mu$ captures the true strain rate dependence of shear stress of a Bingham fluid more faithfully, it has been decided to use $\mu_{\text{yield}} = 10^4\mu$ for all the simulations.

The isotherms become increasingly curved with the strengthening of advection with increasing Ra_{CWHF}, which can be confirmed from the rising magnitude of Ψ with increasing Ra_{CWHF}. A comparison between $\text{Bn}_{CWHF} = 0$ and $\text{Bn}_{CWHF} = 0.25$ cases reveals that the isotherms for Bingham fluid are less curved than the Newtonian case for the same nominal value of Rayleigh number. This behavior is a consequence of weaker advection strength in Bingham fluids than in the Newtonian case for the same nominal value of Ra_{CWHF}, which can be confirmed from the smaller magnitude of Ψ in the Bingham case than in the Newtonian case for a given value of Ra_{CWHF}. Due to increased flow resistance in Bingham fluids the effects of convection are felt at higher values of Ra_{CWHF} than that in Newtonian fluids. For example, convection becomes strong enough to make the isotherms curved for Newtonian fluids at $\text{Ra}_{CWHF} = 5 \times 10^3$, whereas at the same value of nominal Rayleigh number the isotherms remain parallel to horizontal walls for $\text{Bn}_{CWHF} = 0.25$, indicating conduction-driven thermal transport.

4.2 Effects of Bingham Number

The variations of nondimensional horizontal velocity component U and temperature (i.e., θ_{CWT} and θ_{CWHF}) along the vertical midplane for different Bingham numbers for nominal Rayleigh numbers (i.e., Ra_{CWT} and Ra_{CWHF}) equal to 1×10^4 and 1×10^5 are shown in Fig. 4. It is evident from Fig. 4 that the magnitude of U decreases with increasing Bingham number for a given Rayleigh number for both CWT and CWHF boundary conditions because the effects of flow resistance strengthen with increasing Bingham number. The decrease in U magnitude leads to weakening of thermal advection which gives rise to the decrease in the extent of nonlinearity of the temperature variation along the vertical direction. Figure 4 shows that the thermal boundary-layer thickness δ_{th} increases with increasing Bingham number for both CWT and CWHF boundary conditions as indicated by Eqs. (12) and (13). The increase in the thermal boundary-layer thickness δ_{th} with increasing Bingham number leads to reduced nonlinearity of the temperature variation along the vertical direction. The decrease in nonlinearity of temperature variation along the vertical direction with increasing Bingham number indicates that conduction plays an increasingly important role in thermal transport with increasing Bingham number. For large values of Bingham number the heat transfer takes place purely due to thermal conduction because under that condition fluid flow either stops or becomes weak enough to impart considerable influence on the thermal transport within the enclosure. The conduction-driven thermal transport is reflected in the linear variation of temperature in the vertical direction. As the thermal boundary-layer thickness δ_{th} increases with increasing Bn_{CWHF}, the magnitude of $\theta_{CWHF} \sim \delta_{th}/L$ also increases with increasing Bingham number in the case of the CWHF boundary condition. For large values of Bingham number the heat transfer takes place due to conduction and under pure conduction the temperature distributions for both the CWT and CWHF boundary conditions become equal to each other. Thus the distributions of θ_{CWT} and θ_{CWHF} approach each other with increasing Bingham number for a given numerical value of Rayleigh number. Comparing flows under nominal Rayleigh number (i.e., Ra_{CWT} and Ra_{CWHF}) equal to 1×10^4 and 1×10^5 indicates that advective transport strengthens with increasing Rayleigh number which is reflected in the higher magnitude of U as suggested by Eqs. (8a) and (8b). The above behavior can be substantiated from the contours of θ_{CWHF} and Ψ at $\text{Ra}_{CWHF} = 10^4$ and 10^5 in Fig. 5 for Pr = 10 for the CWHF boundary condition. The corresponding variations for the CWT boundary condition are not explicitly shown here because of their qualitative similarities to the CWHF boundary condition. It can be seen from Fig. 5 that the magnitude of Ψ decreases with increasing Bingham number due to weakening of fluid motion and this is reflected in the increased size of AURs for higher values of Bn_{CWHF}. At high values of Bn_{CWHF} the whole enclosure becomes an AUR and under this condition the fluid flow becomes too weak to influence the heat transfer and thus the heat transfer takes place solely due to thermal

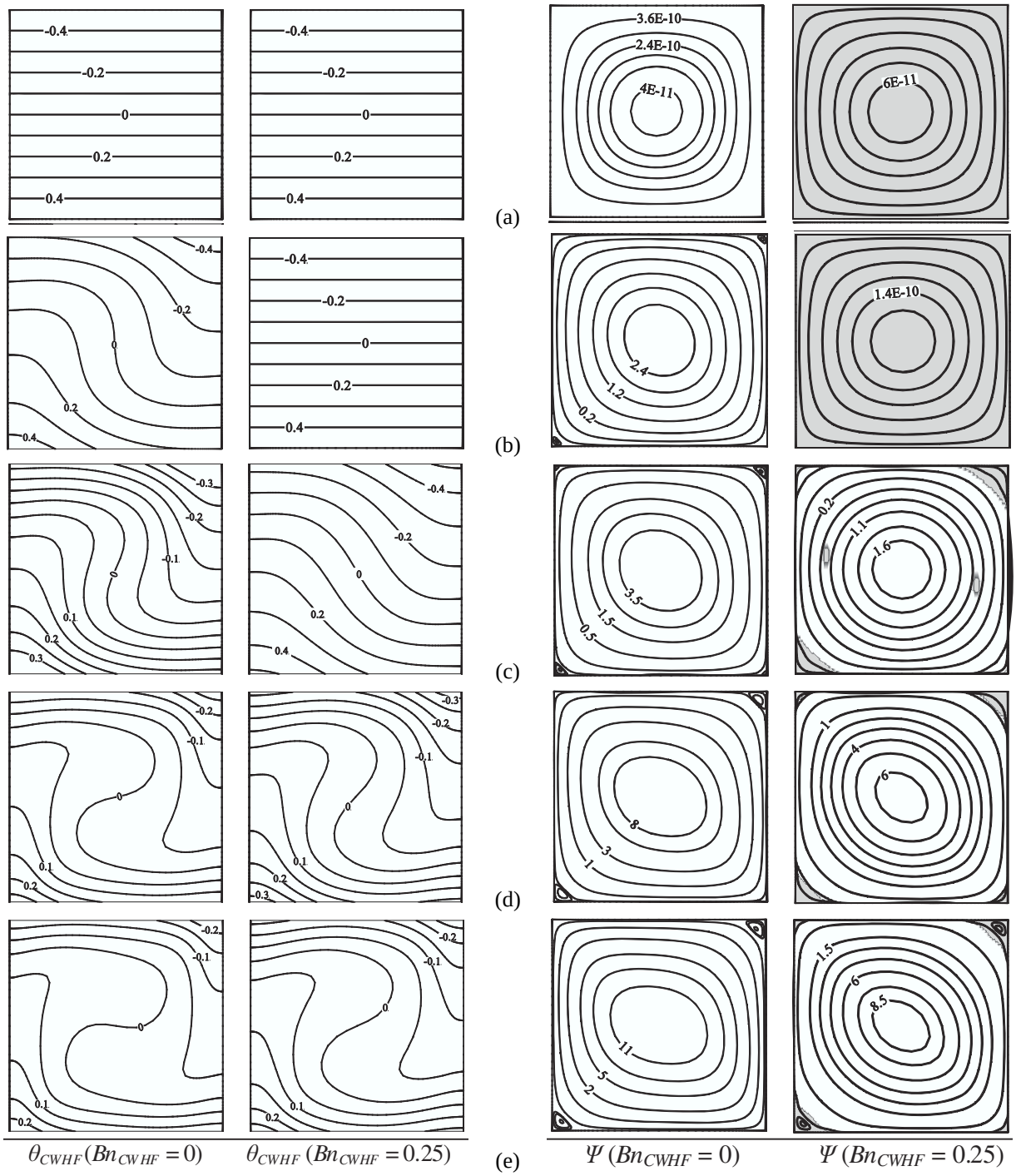

FIG. 3: Contours of nondimensional temperature θ_{CWHF}, stream function Ψ, and unyielded zones (gray) for Newtonian fluid and Bingham fluid at Pr = 10 for Ra_{CWHF} = **(a)** 1×10^3, **(b)** 5×10^3, **(c)** 1×10^4, **(d)** 5×10^4, and **(e)** 1×10^5.

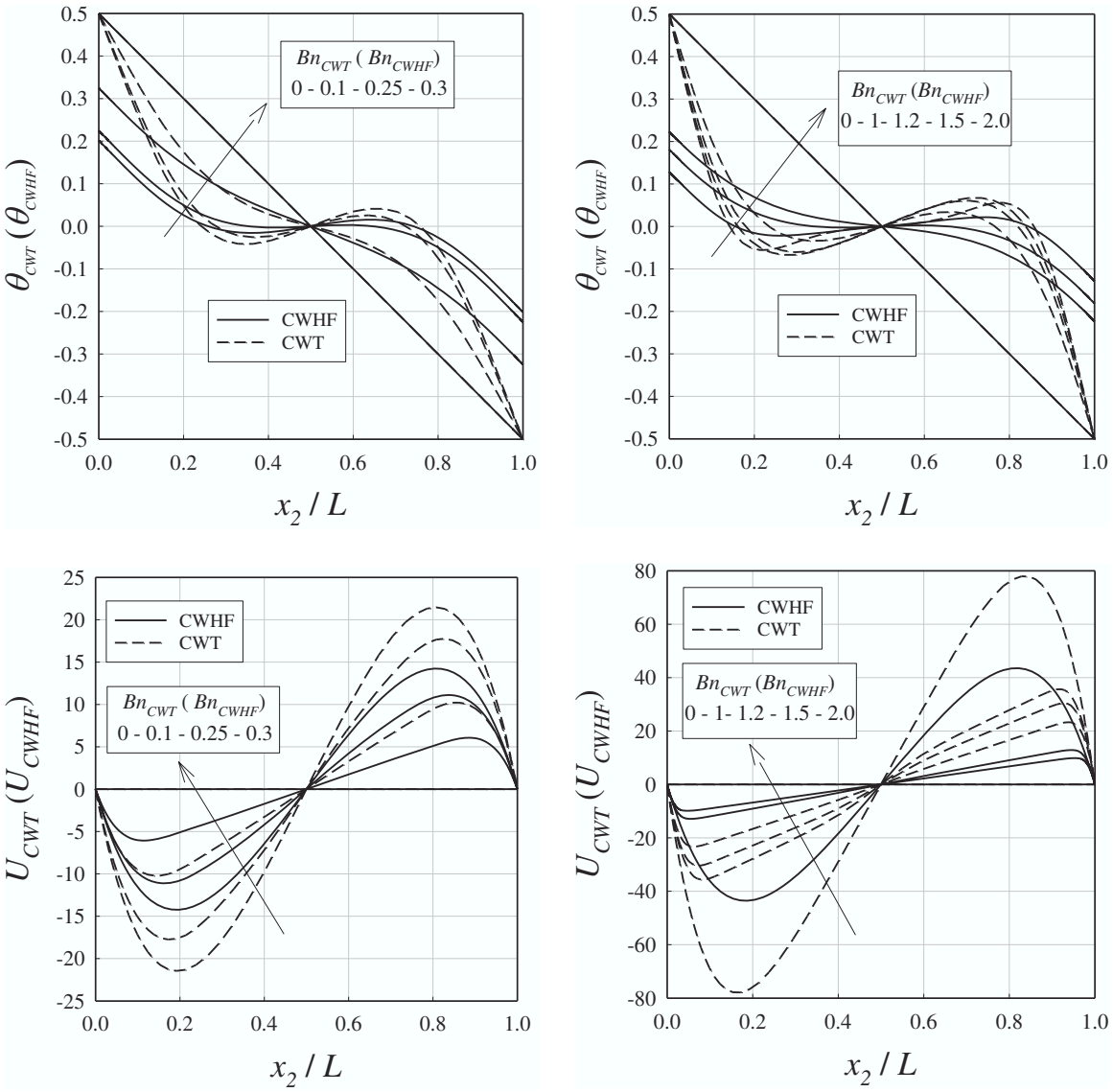

(a) (b)

FIG. 4: Variations of nondimensional temperature θ_{CWT} (θ_{CWHF}) and horizontal velocity component U_{CWT} (U_{CWHF}) along the vertical midplane (i.e., along x_1/L = 0.5) for Bingham fluids at Pr = 10 for $\mathrm{Ra}_{CWT}(\mathrm{Ra}_{CWHF}) =$ **(a)** 1×10^4, **(b)** 1×10^5.

conduction. This pure-conduction limit is reflected in the parallel horizontal isotherms in Fig. 5. The isotherms become increasingly curved with decreasing Bn_{CWHF} due to strengthening of advective transport. Due to stronger advective transport at higher values of Rayleigh number, the flow can resist the effects of yield stress up to a higher value of Bingham number. Thus the Bingham number at which the temperature profile becomes linear along the vertical direction (i.e., fluid flow is too weak to influence thermal transport) increases with increasing Rayleigh number for both CWT and CWHF boundary conditions. It has been noted earlier that the effects of advection are stronger for the CWT boundary condition than in the case of the CWHF boundary condition and thus the

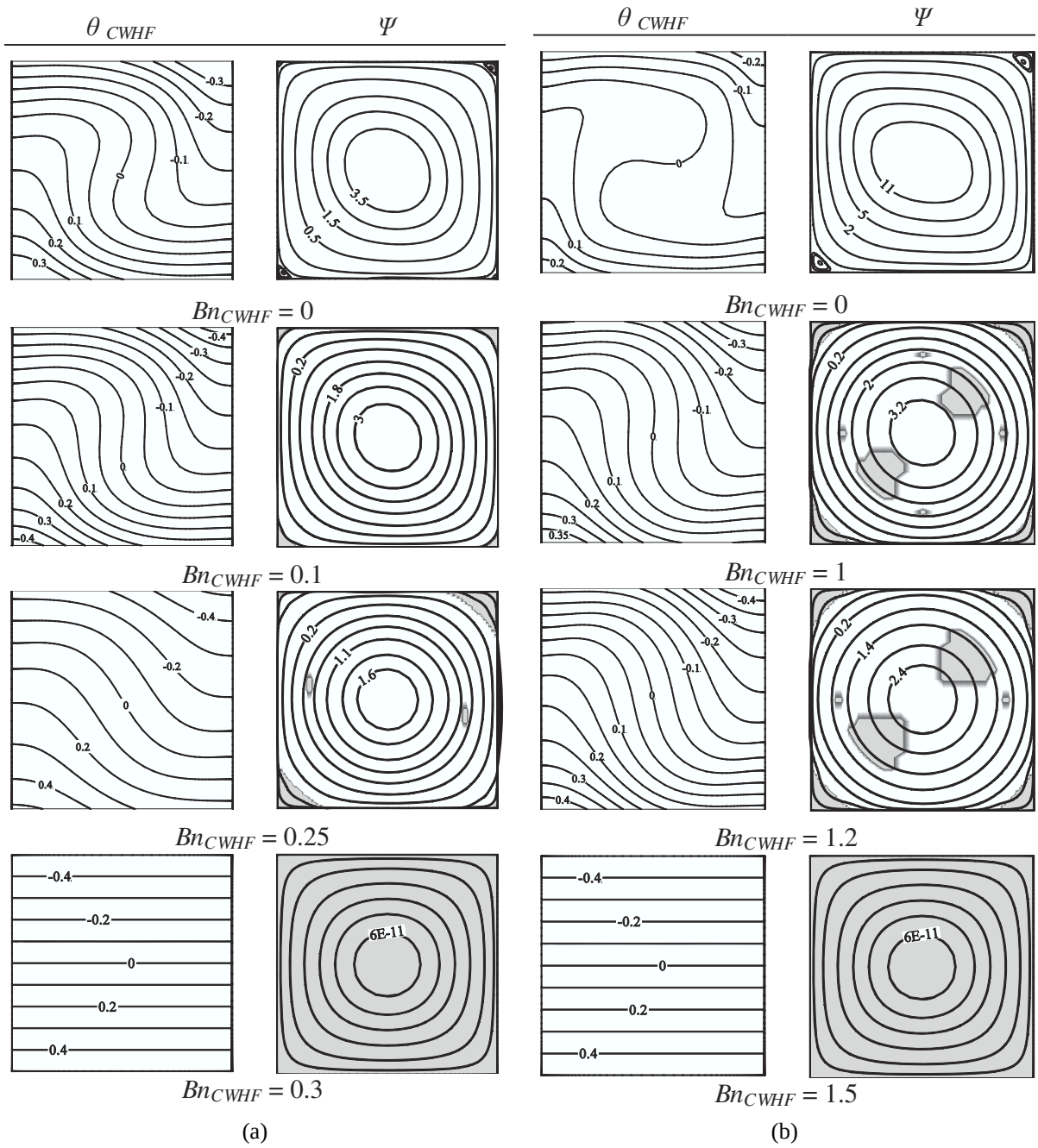

FIG. 5: Contours of nondimensional temperature θ_{CWHF}, stream function Ψ, and unyielded zones (gray) for Bingham fluids for the CWHF boundary condition at Pr = 10 for $\mathrm{Ra}_{CWHF} =$ **(a)** 1×10^4, **(b)** 1×10^5.

fluid flow within the enclosure resists the effects of additional flow resistance due to yield stress up to a higher value of Bingham number in case of the CWT boundary condition than in the CWHF boundary condition. It can be seen from Fig. 4 that it is possible to have nonlinear temperature distribution along the vertical direction for the CWT boundary condition for a Bingham number Bn_{CWT} for which temperature distribution is linear along the x_1

direction for the CWHF boundary condition for the same numerical value of Bingham number Bn_{CWHF}. This tendency is particularly prevalent for high values of Rayleigh number (e.g., $\mathrm{Ra}_{CWT} = \mathrm{Ra}_{CWHF} = 10^5$) where the effects of advection are prominent.

4.3 Behavior of Mean Nusselt Number $\overline{\mathrm{Nu}}$

The effects of Pr on the mean Nusselt number $\overline{\mathrm{Nu}}$ for Newtonian fluids (i.e., Bn_{CWT} = 0 and Bn_{CWHF} = 0) are shown in Fig. 6, which shows $\overline{\mathrm{Nu}}$ slightly increases between Pr = 0.1 and 1.0 but the change in $\overline{\mathrm{Nu}}$ is marginal between Pr = 1.0 and 1000. The heat transfer characteristics in the present configuration depend on the relative strengths of inertial, viscous, and buoyancy forces. For small values of Pr the thermal boundary-layer thickness remains much greater than the hydrodynamic boundary-layer thickness and thus the inertial and buoyancy forces principally govern the transport behavior. In contrast, for large values of Pr the hydrodynamic boundary-layer thickness remains much greater than the thermal boundary-layer thickness, thus the transport characteristics are primarily governed by buoyancy and viscous forces [see the scaling analysis by Bejan (1984)]. For Pr $\ll$ 1, an increase in Pr decreases the thermal boundary-layer thickness in comparison to the hydrodynamic boundary-layer thickness, which acts to increase the heat flux which is reflected in the increasing Nusselt number. In the case of Pr $\gg$ 1, a change in Prandtl number modifies the relative balance between viscous and buoyancy forces so the heat transport in the thermal boundary layer gets only marginally affected. This modification is reflected in the weak Prandtl number dependence of $\overline{\mathrm{Nu}}$ for large values of Pr (i.e., Pr $\gg$ 1) for both CWT and CWHF boundary conditions in Fig. 6.

The heat transfer coefficient h can be scaled as $h = q/\Delta T \sim k\Delta T/\Delta T\delta_{th} \sim k/\delta_{th}$ and thus the mean Nusselt number $\overline{\mathrm{Nu}}$ can be taken to scale as $\overline{\mathrm{Nu}} = hl/k \sim L/\delta_{th}$ (Turan et al., 2010, 2011). Using Eqs. (12) and (13) one can obtain the following $\overline{\mathrm{Nu}}$ in Newtonian fluids (i.e., $\mathrm{Bn}_{CWT} = 0$ and $\mathrm{Bn}_{CWHF} = 0$):

$$\overline{\mathrm{Nu}} \sim (\mathrm{Ra}_{CWT}/\mathrm{Pr})^{1/4} f_3(\mathrm{Ra}_{CWT}, \mathrm{Pr})(CWT) \quad \text{and}$$
$$\overline{\mathrm{Nu}} \sim (\mathrm{Ra}_{CWHF}/\mathrm{Pr})^{1/5} f_4^{0.8}(\mathrm{Ra}_{CWHF}, \mathrm{Pr}) \times (CWHF) \tag{14}$$

Equation (14) suggests that $\overline{\mathrm{Nu}}$ values are likely to be different between the CWT and CWHF configurations for the same numerical value of Ra_{CWT} and Ra_{CWHF}. For small values of Ra_{CWT} and Ra_{CWHF} the values of $\overline{\mathrm{Nu}}$ are comparable in both CWT and CWHF boundary conditions. For large values of Rayleigh number the difference between $(\mathrm{Ra}_{CWT}/\mathrm{Pr})^{1/4}$ and $(\mathrm{Ra}_{CWHF}/\mathrm{Pr})^{1/5}$ widens and that is reflected in the value of $\overline{\mathrm{Nu}}$ being smaller in the CWHF case than that in the CWT case for the same numerical values of Rayleigh and Prandtl numbers as can be observed from Fig. 6. It has been demonstrated earlier that the strength of advection is stronger in the CWT case than in the CWHF case for the same values of Rayleigh and Prandtl numbers [see Eqs. (8a) and (8b)] and this is reflected in the value of $\overline{\mathrm{Nu}}$ being greater in the CWT case than in the CWHF case. The simulation results for the CWT boundary condition are also in agreement with previous findings (Corcione, 2003; Quertatani et al., 2008).

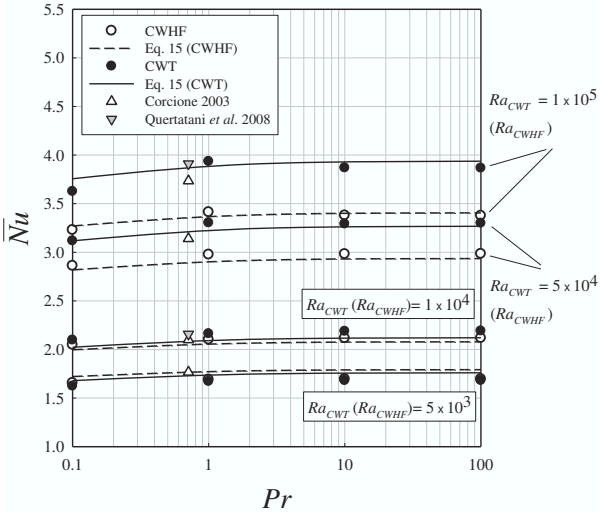

FIG. 6: Variation of mean Nusselt number $\overline{\mathrm{Nu}}$ with Rayleigh $\mathrm{Ra}_{CWT}(\mathrm{Ra}_{CWHF})$ and Prandtl Pr numbers for Newtonian fluids.

In the present study a correlation for the mean Nusselt number $\overline{\mathrm{Nu}}$ for Newtonian fluids is proposed in the following manner for $10^5 \geq \mathrm{Ra}_{CWT} \geq 5 \times 10^3$ ($10^5 \geq \mathrm{Ra}_{CWHF} \geq 5 \times 10^3$):

$$\overline{\mathrm{Nu}} = a\mathrm{Ra}_{CWT}^m \left(\frac{\mathrm{Pr}}{1+\mathrm{Pr}}\right)^n \quad \text{and}$$
$$\overline{\mathrm{Nu}} = a\mathrm{Ra}_{CWHF}^m \left(\frac{\mathrm{Pr}}{1+\mathrm{Pr}}\right)^n \tag{15a}$$

The values of the coefficients *a*, *m*, and *n* were determined by an iterative minimization function of a commercial software package which provides the following values:

$a = 0.178,\ m = 0.269,\ n = 0.02$ for CWT;
$a = 0.289,\ m = 0.214,\ n = 0.017$ for CWHF (15b)

For the parameters given by Eq. (15b), the correlation given by Eq. (15a) satisfactorily captures the variation of $\overline{\text{Nu}}$ in the range given by $5 \times 10^3 \leq \text{Ra}_{CWT} \leq 10^5$, $5 \times 10^3 \leq \text{Ra}_{CWHF} \leq 10^5$, and $0.1 \leq \text{Pr} \leq 10^3$ for Newtonian fluids. The correlation given by Eq. (15a) is in good agreement with the scaling estimates given by Eq. (14) and the small difference in the exponent of Rayleigh number between Eqs. (14) and (15a) are not unexpected given the simplicity of the scaling relations.

The variation of $\overline{\text{Nu}}$ with Bingham number for different values of Rayleigh number at Pr = 10 are shown in Fig. 7 (the cases corresponding to $\text{Ra}_{CWT} = 10^3$ and $\text{Ra}_{CWHF} = 10^3$ are not shown because the mean Nusselt number $\overline{\text{Nu}}$ remains equal to unity for all fluids). The results shown in Fig. 7 are primarily obtained from the biviscosity regularization but the use of the Papanastasiou model (1987) was found to give virtually identical results. The variation in Nusselt number between the regularization methods for nominally identical conditions was usually smaller than 0.1% and small differences became apparent only at large Bingham numbers, when the Nusselt number approaches unity (still less than 3% in $\overline{\text{Nu}}$). Thus these differences are, for all practical purposes, unimportant for the following discussion. Figure 7 indicates that $\overline{\text{Nu}}$ decreases with increasing Bingham number. An increase in Bingham number implies that higher stress needs to be created to induce fluid motion and thus thermal convection within the enclosure. This increased flow resistance at higher values of Bingham number gives rise to weaker thermal convection in the enclosure, which is reflected in the small values of $\overline{\text{Nu}}$ for high values of Bingham number. It can be seen from Fig. 7 that $\overline{\text{Nu}}$ at a given set of values of Rayleigh and Prandtl numbers decreases with increasing Bingham number before dropping to $\overline{\text{Nu}}$ = 1.0 at a Bingham number $\text{Bn}_{\max}$ such that $\overline{\text{Nu}}$ remains equal to unity for $\text{Bn}_{CWT} \geq \text{Bn}_{\max}$ ($\text{Bn}_{CWHF} \geq \text{Bn}_{\max}$). It has been discussed earlier that δ_{th} increases with increasing Bingham number for both CWT and CWHF boundary conditions [see Eqs. (12) and (13)], which leads to a decrease in $\overline{\text{Nu}}$ with increasing Bingham number as $\overline{\text{Nu}}$ scales as $\overline{\text{Nu}} \sim L/\delta_{th}$ (Turan et al., 2010, 2011). Figure 7 shows that the mean Nusselt number $\overline{\text{Nu}}$ increases with increasing Rayleigh number for a given set of values of Prandtl and Bingham numbers for $\text{Bn}_{CWT} < \text{Bn}_{\max}$ ($\text{Bn}_{CWHF} < \text{Bn}_{\max}$), which is also consistent with the scaling estimates of δ_{th} [see Eqs. (12) and (13)] suggesting a decrease in δ_{th} with increasing Rayleigh number for a given set of values of Bingham and Prandtl numbers. An increase in Rayleigh number gives rise to strengthening of convection for a given set of values of Prandtl and Bingham numbers for $\text{Bn}_{CWT} < \text{Bn}_{\max}$ ($\text{Bn}_{CWHF} < \text{Bn}_{\max}$) and this is reflected in the high values of $\overline{\text{Nu}}$ for high values of Ra_{CWT} (Ra_{CWHF}). Stronger fluid flow at higher values of Rayleigh number can resist the flow resistance up to

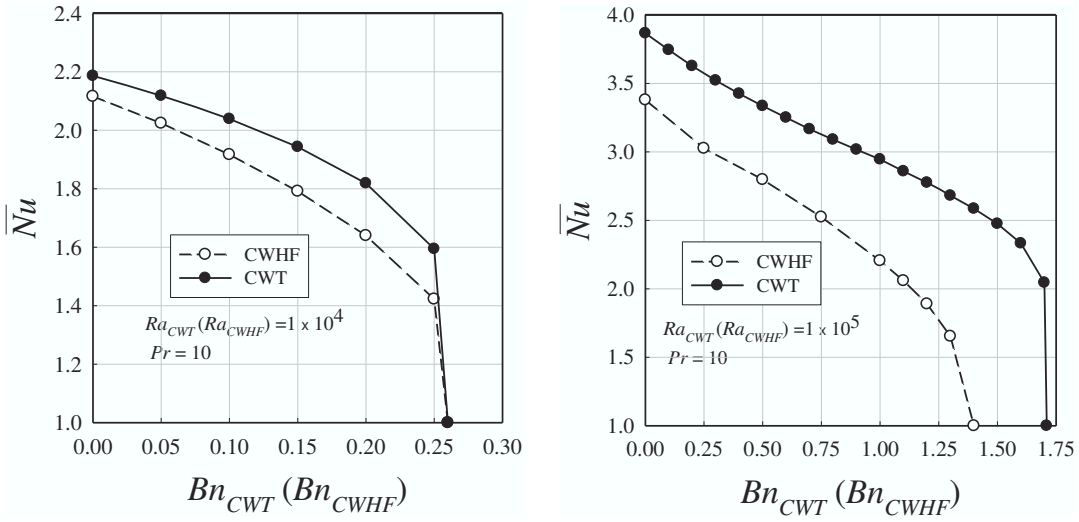

FIG. 7: The interrelation between the mean Nusselt number $\overline{\text{Nu}}$ and Bingham number $\text{Bn}_{CWT}(\text{Bn}_{CWHF})$ at Pr = 10 for $\text{Ra}_{CWT}(\text{Ra}_{CWHF}) =$ **(a)** 1×10^4 and **(b)** 1×10^5.

greater values of Bingham number which gives rise to an increase in $\mathrm{Bn}_{\max}$ with increasing Rayleigh number for a given value of Prandtl number for both CWT and CWHF boundary conditions. It is worth noting that the variation of the mean Nusselt number with Bingham number in the case of natural convection of Bingham fluids in rectangular enclosures with differentially heated vertical sidewalls (Turan et al., 2010, 2011) is quantitatively and qualitatively different from the results presented here.

As $\overline{\mathrm{Nu}}$ for Newtonian fluids in the case of the CWHF boundary condition remains smaller than that in the case of the CWT boundary condition, the Nusselt number in Bingham fluids also assumes a smaller value in the case of the CWHF boundary condition than in the CWT boundary condition for the same numerical values of Rayleigh, Bingham, and Prandtl numbers (see Fig. 7). Moreover, Fig. 7 indicates that $\mathrm{Bn}_{\max}$ in the CWHF case assumes smaller values than in the case of the CWT boundary condition. This is unlike the natural convection of Bingham fluids in enclosures with differentially heated vertical side walls where $\mathrm{Bn}_{\max}$ for both CWT and CWHF boundary conditions were found to be the same (Turan et al., 2011). In differentially heated sidewalls fluid flow within the enclosure initiates as soon as a finite temperature difference is induced between the vertical walls (Bejan, 1984). Thus the fluid flow progressively weakens and ceases to influence the heat transfer rate by advection as the Bingham number increases in the differentially heated side wall configuration, which is reflected in a linear temperature distribution between vertical sidewalls (Turan et al., 2011). Under that situation, the temperature distributions for the CWT and CWHF boundary conditions approach the pure-conduction solution and the definitions of nominal Rayleigh and Bingham numbers become equivalent to each other (i.e., $\mathrm{Ra}_{CWT} = \mathrm{Ra}_{CWHF}$ and $\mathrm{Bn}_{CWT} = \mathrm{Bn}_{CWHF}$), which in turn leads to the same numerical value of $\mathrm{Bn}_{\max}$ for differentially heated vertical side walls (Turan et al., 2011). By contrast, the Rayleigh number in the RB configuration must exceed a critical limit Ra_{crit} before any fluid flow is induced within the enclosure and any noticeable influence is felt on the mean Nusselt number $\overline{\mathrm{Nu}}$ (Bejan, 1984). The actual Rayleigh number in Bingham fluids is a local quantity and can assume very different values in comparison to its nominal value because the effective viscosity in Bingham fluid changes from one point to another. An effective viscosity μ_{eff} can be estimated as

$$\mu_{\mathrm{eff}} \sim \mu[\tau_y \delta/\mu\vartheta + 1] \tag{16}$$

Using $\vartheta \sim \sqrt{g\beta(T_H - T_C)L}$ and $\vartheta \sim \sqrt{g\beta q \delta_{th} L/k}$ in the CWT and CWHF configurations, respectively, yields the following scaling of μ_{eff}/μ:

$$\mu_{\mathrm{eff}}/\mu \sim [\mathrm{Bn}_{CWT} f_3(\mathrm{Ra}_{CWT}, \mathrm{Bn}_{CWT}, \mathrm{Pr})(\delta_{th}/L) + 1] \quad \text{(for CWT)} \tag{17a}$$

$$\mu_{\mathrm{eff}}/\mu \sim [\mathrm{Bn}_{CWHF} f_4(\mathrm{Ra}_{CWHF}, \mathrm{Bn}_{CWHF}, \mathrm{Pr}) \times (\delta_{th}/L)^{1/2} + 1] \quad \text{(for CWHF)} \tag{17b}$$

Using Eqs. (17a) and (17b) for the CWT and CWHF boundary conditions, respectively, gives rise to

$$\mathrm{Ra}_{\mathrm{eff}} = \rho g \beta (T_H - T_C) L^3/\mu_{\mathrm{eff}}\alpha \sim \mathrm{Ra}_{CWT}/[\mathrm{Bn}_{CWT} \times f_3(\mathrm{Ra}_{CWT}, \mathrm{Bn}_{CWT}, \mathrm{Pr})(\delta_{th}/L) + 1] \quad \text{(for CWT)} \tag{18a}$$

$$\mathrm{Ra}_{\mathrm{eff}} = \rho g \beta q L^4/k\mu_{\mathrm{eff}}\alpha \sim \mathrm{Ra}_{CWHF}/[\mathrm{Bn}_{CWHF} \times f_4(\mathrm{Ra}_{CWHF}, \mathrm{Bn}_{CWHF}, \mathrm{Pr})(\delta_{th}/L)^{1/2} + 1] \quad \text{(for CWHF)} \tag{18b}$$

Assuming f_3 and f_4 attain similar values for a given set of numerical values of nominal Rayleigh, Bingham, and Prandtl numbers, it can be inferred from Eqs. (18a) and (18b) that $\mathrm{Ra}_{\mathrm{eff}}$ in the CWHF boundary condition is likely to assume a smaller value than in the CWT configuration for a given set of numerical values of nominal Rayleigh, Bingham, and Prandtl numbers because $\delta_{th}/L < 1$ and δ_{th} is greater in the CWHF case than in the CWT case due to a smaller value of $\overline{\mathrm{Nu}}$ in the CWHF configuration. This indicates that $\mathrm{Ra}_{\mathrm{eff}}$ decays more rapidly with increasing Bingham number in the CWHF case than in the CWT case for a given set of values of nominal Rayleigh and Prandtl numbers. Once $\mathrm{Ra}_{\mathrm{eff}}$ becomes smaller than Ra_{crit}, conduction becomes the primary mechanism of heat transfer which is reflected in the unity value of mean Nusselt number $\overline{\mathrm{Nu}}$. This situation is encountered at a smaller value of nominal Bingham number in the CWHF case than in the CWT case for high values of nominal Rayleigh number (e.g., $\mathrm{Ra}_{CWT} = \mathrm{Ra}_{CWHF} = 10^5$ in Fig. 7) where $\delta_{th} \ll L$ for small values of Bingham number. This leads to a smaller value of $\mathrm{Bn}_{\max}$ (i.e., the Bingham number below which $\overline{\mathrm{Nu}}$ assumes a value greater than unity) in the CWHF case than in the CWT case for high values of nominal Rayleigh number. For small values of Rayleigh number $\delta_{th}/L \sim O(1)$, and thus the values of $\mathrm{Ra}_{\mathrm{eff}}$ remain comparable for both CWT and CWHF boundary conditions, which give rise to comparable values of $\mathrm{Bn}_{\max}$ for

the CWT and CWHF boundary conditions at small values of nominal Rayleigh number (i.e., $\mathrm{Ra}_{CWT} = \mathrm{Ra}_{CWHF} = 10^4$ in Fig. 7).

The variations of $\overline{\mathrm{Nu}}$ with Bingham number for different Prandtl numbers at $\mathrm{Ra}_{CWT} = \mathrm{Ra}_{CWHF} = 10^4$ are shown in Fig. 8, which show that unlike Newtonian fluids the mean Nusselt number $\overline{\mathrm{Nu}}$ decreases with increasing Pr for large values of Bingham number for both CWT and CWHF boundary conditions. However, for small values of Bingham number the mean Nusselt number $\overline{\mathrm{Nu}}$ increases with increasing Pr for very small values of Bingham number, which is consistent with the behavior obtained for Newtonian fluids (see Fig. 6). Moreover, the value of Bingham number $\mathrm{Bn}_{\max}$ for which $\overline{\mathrm{Nu}}$ approaches unity decreases with increasing Pr. The same qualitative behavior is also observed for other values of Rayleigh number. This variation clearly demonstrates that $\mathrm{Bn}_{\max}$ depends on Pr for a given value of Rayleigh number, which can be confirmed from inspection of Table 3 where the values of $\mathrm{Bn}_{\max}$ are estimated here by carrying out simulations and identifying the Bingham number at which $\overline{\mathrm{Nu}}$ obtains a value of 1.01 (i.e., $\overline{\mathrm{Nu}} = 1.01$).

From the foregoing it can be concluded that the effects of Pr on natural convection at a given value of Rayleigh number are not fully independent of Bingham number. This inference is an artifact of how the nominal Rayleigh number is defined in the present analysis [see Eq. (5a)]. Following Eqs. (17) and (18) it is possible to estimate an effective Grashof number $\mathrm{Gr}_{\mathrm{eff}}$ in the following manner:

$$\mathrm{Gr}_{\mathrm{eff}} = \rho^2 g\beta(T_H - T_C)L^3/\mu_{\mathrm{eff}}^2 \sim \mathrm{Ra}_{CWT}\mathrm{Pr}^{-1} /[\mathrm{Bn}_{CWT} f_3(\mathrm{Ra}_{CWT}, \mathrm{Bn}_{CWT}, \mathrm{Pr})(\delta_{th}/L) + 1]^2 \quad \text{(for CWT)} \tag{19a}$$

$$\mathrm{Gr}_{\mathrm{eff}} = \rho^2 g\beta q L^4/k\mu_{\mathrm{eff}}^2 \sim \mathrm{Ra}_{CWHF}\mathrm{Pr}^{-1} /[\mathrm{Bn}_{CWHF} f_4(\mathrm{Ra}_{CWHF}, \mathrm{Bn}_{CWHF}, \mathrm{Pr})(\delta_{th}/L)^{1/2}+1]^2 \quad \text{(for CWHF)} \tag{19b}$$

It has been shown δ_{th}/L increases with increasing Bingham number for both CWT and CWHF boundary conditions, as $\overline{\mathrm{Nu}} \sim L/\delta_{th}$ decreases with increasing Bingham number (see Fig. 7). Moreover f_3 and f_4 are expected to increase with increasing Pr which suggests that an increase in Prandtl number leads to a large drop in $\mathrm{Gr}_{\mathrm{eff}}$ for large values of Bingham number. This suggests that the effects of the buoyancy force become increasingly weak in comparison to the viscous effects with increasing Pr for large values of nominal Bingham number when the nominal Rayleigh number is held constant. This weakened

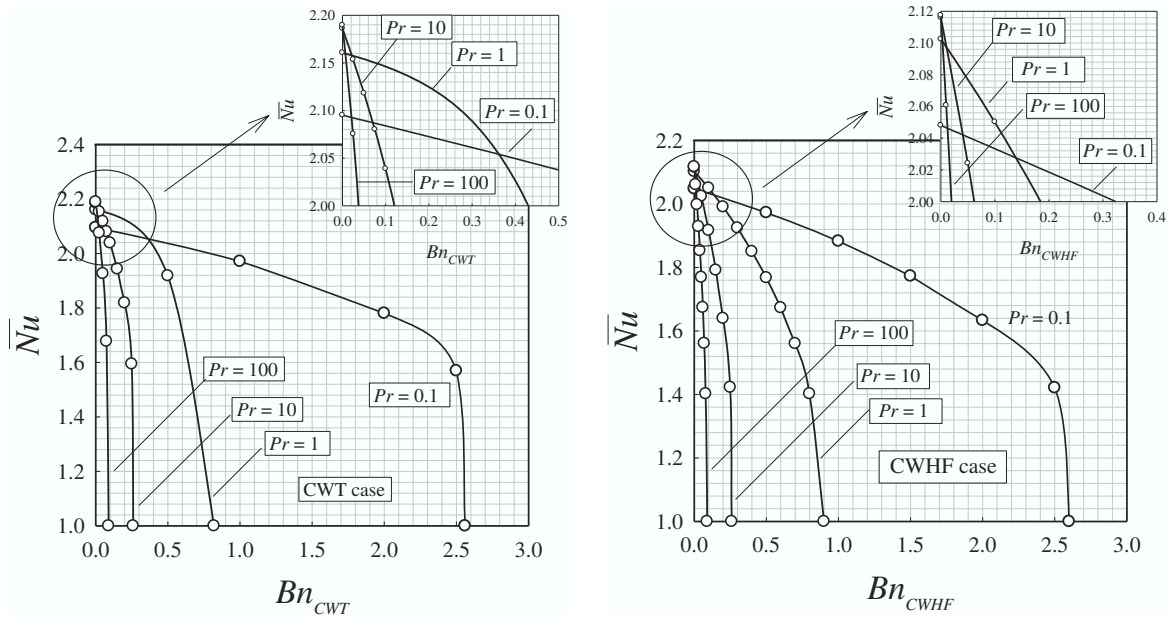

FIG. 8: Variations of mean Nusselt number $\overline{\mathrm{Nu}}$ with Prandtl number for Bingham fluids at $\mathrm{Ra}_{CWT}(\mathrm{Ra}_{CWHF}) = 10^4$ for **(a)** CWT and **(b)** CWHF boundary conditions.

TABLE 3: Values of $\mathrm{Bn_{max}}$ at different values of Rayleigh and Prandtl numbers

$\mathbf{Ra_{CWT}}$ ($\mathbf{Ra_{CWHF}}$)	$\mathbf{5\times10^3}$		$\mathbf{1\times10^4}$		$\mathbf{5\times10^4}$		$\mathbf{1\times10^5}$	
Pr	**CWT**	**CWHF**	**CWT**	**CWHF**	**CWT**	**CWHF**	**CWT**	**CWHF**
0.1	0.83	1.19	2.56	2.62	10.86	8.85	17.06	13.32
1	0.27	0.38	0.82	0.83	3.44	2.80	5.40	4.22
10	0.09	0.12	0.26	0.27	1.09	0.89	1.71	1.34
100	0.03	0.04	0.09	0.09	0.35	0.28	0.54	0.40

buoyancy force relative to the viscous force gives rise to a weakening of advective transport which acts to decrease $\overline{\mathrm{Nu}}$ with increasing Pr. This effect is relatively weak for small values of nominal Bingham number where an increase in Pr acts to reduce the thermal boundary-layer thickness which in turn acts to increase the heat transfer rate as discussed earlier in the context of Newtonian fluids. In contrast, for large values of nominal Bingham number, the effects of thinning of the thermal boundary-layer thickness with increasing Pr are superseded by the reduction of convective transport strength due to a smaller value of $\mathrm{Gr_{eff}}$. This reduction gives rise to a decrease in $\overline{\mathrm{Nu}}$ with increasing values of Pr (for a given value of nominal Rayleigh number) when the nominal Bingham number attains large values. Eventually this gives rise to the beginning of the conduction-dominated regime for smaller values of $\mathrm{Bn_{max}}$ for higher Pr values as shown in Fig. 8. As a consequence of this, $\mathrm{Bn_{max}}$ depends on both Rayleigh and Prandtl numbers, and $\mathrm{Bn_{max}}$ increases with increasing Rayleigh number, whereas it decreases with increasing Pr (see Table 3).

Using Eq. (12) the mean Nusselt number $\overline{\mathrm{Nu}} \sim L/\delta_{th}$ for Bingham fluids in the CWT boundary condition is given by

$$\overline{\mathrm{Nu}} \sim \max\left\{1, \frac{\mathrm{Ra}_{CWT}^{1/2} f_3(\mathrm{Ra}_{CWT}, \mathrm{Bn}, \mathrm{Pr})}{\mathrm{Pr}^{1/2}} \times \left[\frac{\mathrm{Bn}_{CWT}}{2} + \frac{1}{2}\sqrt{\mathrm{Bn}_{CWT}^2 + 4\left(\frac{\mathrm{Ra}_{CWT}}{\mathrm{Pr}}\right)^{1/2}}\right]^{-1}\right\} \quad (20)$$

Following the above scaling estimate a correlation for $\overline{\mathrm{Nu}}$ can be proposed for the CWT boundary condition:

$$\overline{\mathrm{Nu}} = 1 + \frac{A_{CWT}\mathrm{Ra}_{CWT}^{1/2}}{\left[\frac{\mathrm{Bn}_{CWT}}{2} + \frac{1}{2}\sqrt{\mathrm{Bn}_{CWT}^2 + 4\left(\frac{\mathrm{Ra}_{CWT}}{\mathrm{Pr}}\right)^{1/2}}\right]} \times \left[1 - \left(\frac{\mathrm{Bn}_{CWT}}{\mathrm{Bn}_{\max}}\right)^{0.6}\right]^{b_1} \quad (21)$$

such that $\lim_{\mathrm{Bn_{CWT}}\to\mathrm{Bn_{max}}} \overline{\mathrm{Nu}} = 1.0$ and A_{CWT}, b_1 and $\mathrm{Bn_{max}}$ are input parameters in the correlation. The parameter A_{CWT} needs to be chosen in such a manner that Eq. (21) becomes identically equal to Eq. (15a) when the Bingham number goes to zero (i.e., Newtonian fluid). This gives rise to the following expression for A_{CWT}:

$$A_{CWT} = 0.178\,\mathrm{Ra}_{CWT}^{0.019}\frac{\mathrm{Pr}^{-0.23}}{(1+\mathrm{Pr})^{0.02}} - \frac{1}{\mathrm{Ra}_{CWT}^{0.25}\mathrm{Pr}^{0.25}} \quad (22)$$

The simulation data indicate that the parameter b_1 depends on both Ra_{CWT} and Pr and it has been found that the variation of b_1 with Ra_{CWT} and Pr can be accurately expressed with the help of the following power law:

$$b_1 = 0.025\mathrm{Ra}_{CWT}^{0.171}\mathrm{Pr}^{0.095} \quad (23)$$

It has been discussed earlier that $\mathrm{Bn_{max}}$ is dependent on Ra_{CWT} and Pr and here the value of $\mathrm{Bn_{max}}$ is estimated by empirically fitting the simulation results:

$$\mathrm{Bn_{max}} = [0.0019\ln(\mathrm{Ra}_{CWT}) - 0.0128] \times \mathrm{Ra}_{CWT}^{0.55}\mathrm{Pr}^{-0.50} \quad \text{(for CWT)} \quad (24)$$

The predictions of the correlation given by Eqs. (21)–(24) are compared with $\overline{\mathrm{Nu}}$ obtained from numerical simulations in Fig. 9, which shows that the correlation satisfactorily predicts $\overline{\mathrm{Nu}}$ in the ranges given by $0.1 \le \mathrm{Pr} \le 100$ and $10^4 \le \mathrm{Ra}_{CWT} \le 10^5$.

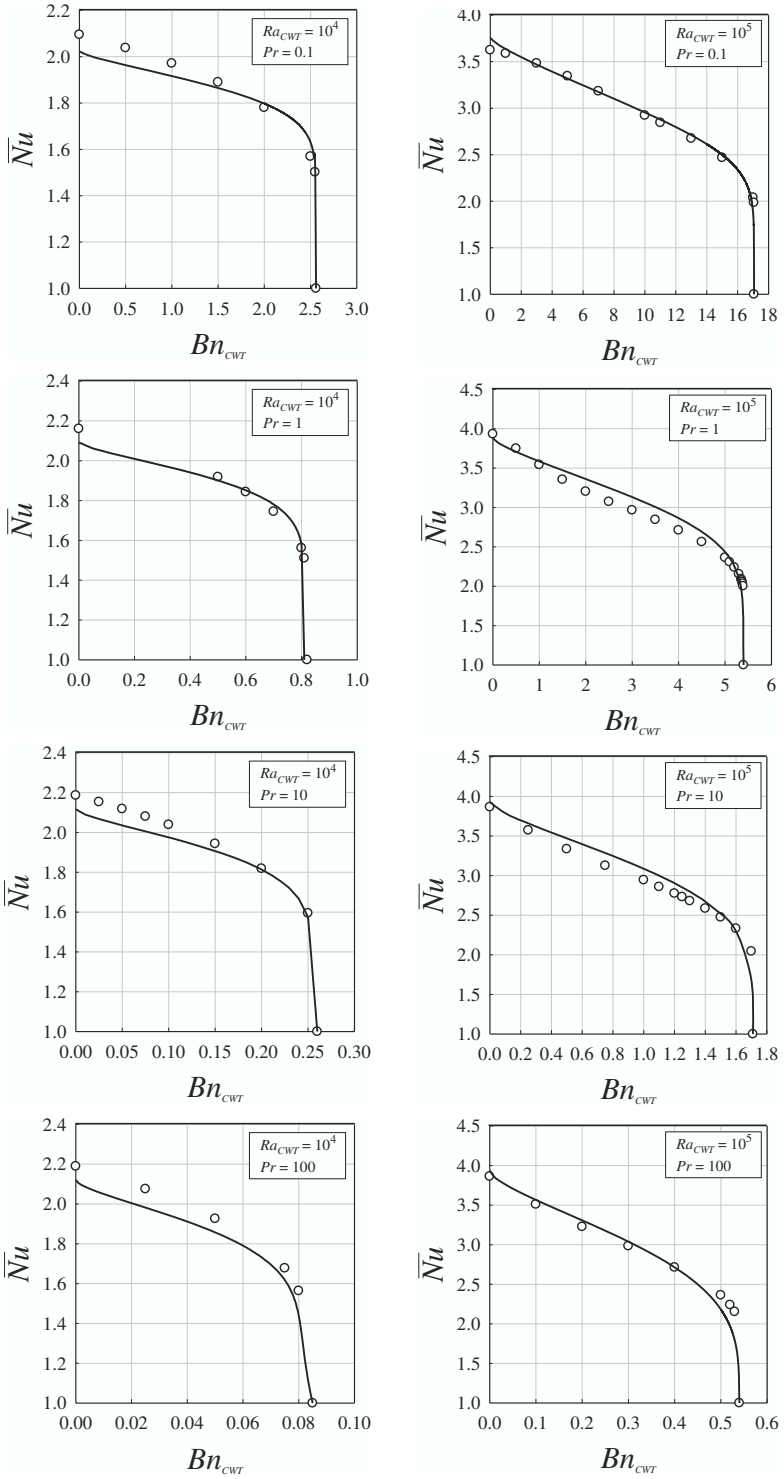

FIG. 9: Comparison of the prediction of the correlation (—) given by Eqs. (21)–(24) and simulation results (○) for CWT case.

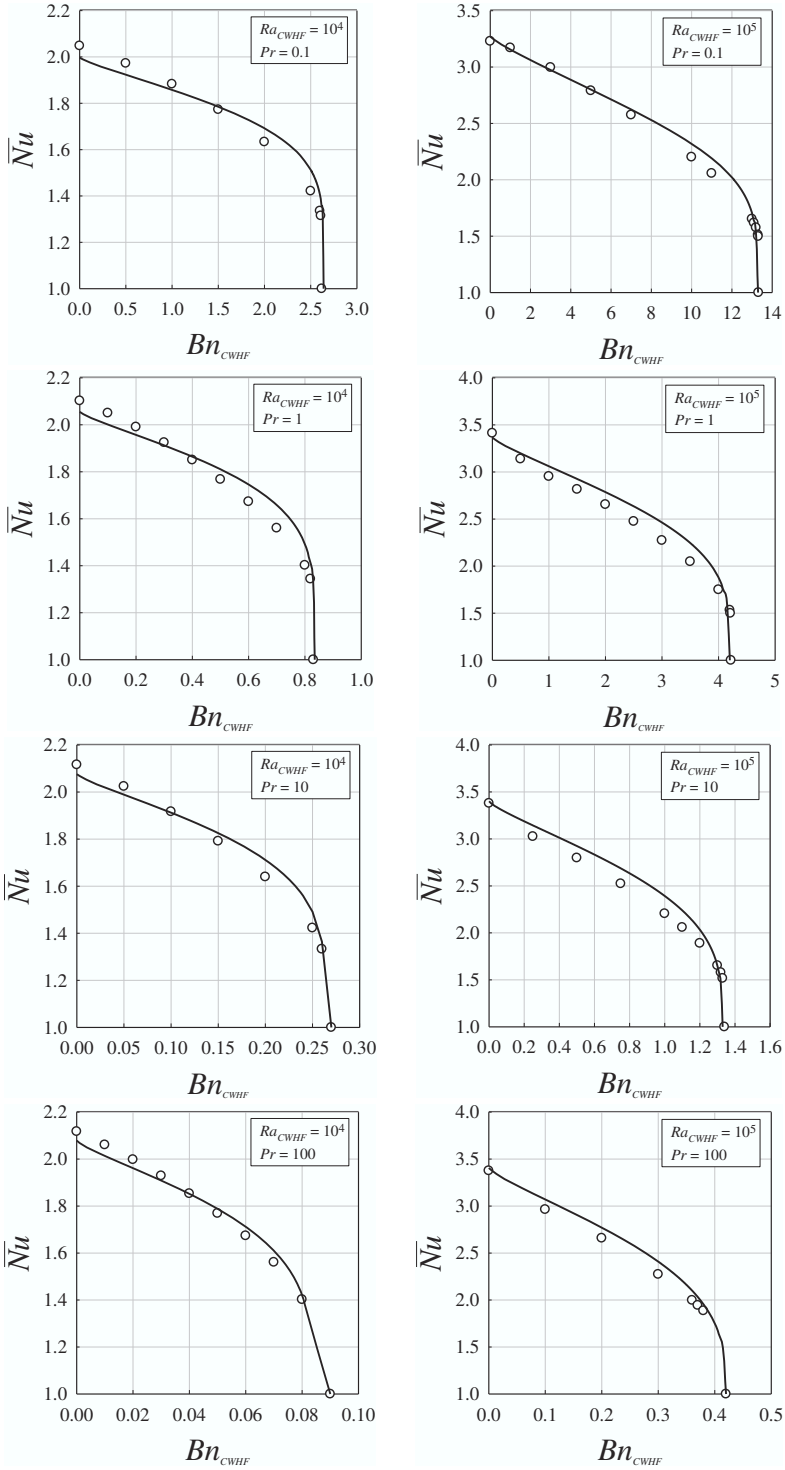

FIG. 10: Comparison of the prediction of the correlation (—) given by Eqs. (25) and (26) and simulation results (○) for CWHF case.

It is difficult to obtain a scaling estimate of δ_{th} from Eq. (13), thus a correlation for $\overline{\text{Nu}}$ is proposed here in the following manner for the CWHF boundary condition considering the qualitative similarities in the Bingham number dependence of mean Nusselt number between CWT and CWHF boundary conditions:

$$\overline{\text{Nu}} = 1 + \frac{A_{CWHF}\text{Ra}_{CWHF}^{1/2}}{\left[\frac{\text{Bn}_{CWHF}}{2} + \frac{1}{2}\sqrt{\text{Bn}_{CWT}^2 + 4\left(\frac{\text{Ra}_{CWHF}}{\text{Pr}}\right)^{1/2}}\right]} \times \left[1 - \left(\frac{\text{Bn}_{CWHF}}{\text{Bn}_{\max}}\right)^{0.75}\right]^{b_2} \quad (25)$$

where

$$A_{CWHF} = 0.205\,\text{Ra}_{CWHF}^{-0.001}\frac{\text{Pr}^{-0.213}}{(1+\text{Pr})^{0.037}} - \frac{1}{\text{Ra}_{CWHF}^{0.25}\text{Pr}^{0.25}} \quad (26a)$$

$$b_2 = 0.0818\text{Ra}_{CWHF}^{0.1019}\text{Pr}^{0.0540} \quad (26b)$$

$$\text{Bn}_{\max} = [0.0412\ln(\text{Ra}_{CWHF}) - 0.3201] \times \text{Ra}_{CWHF}^{0.287}\text{Pr}^{-0.50} \quad \text{(for CWHF)} \quad (26c)$$

The above expression of A_{CWHF} ensures that Eq. (25) becomes exactly equal to Eq. (15a) for Newtonian fluids (i.e., $\text{Bn}_{CWHF} = 0$). Moreover, $\lim_{\text{Bn}_{\text{CWHF}}\to\text{Bn}_{\max}} \overline{\text{Nu}} = 1.0$ according to Eq. (25). The predictions of the correlation given by Eqs. (25) and (26) are compared with $\overline{\text{Nu}}$ obtained from numerical simulations in Fig. 10, which shows that the correlation satisfactorily predicts $\overline{\text{Nu}}$ in the ranges given by $0.1 \le \text{Pr} \le 100$ and $10^4 \le \text{Ra}_{CWHF} \le 10^5$.

5. CONCLUSIONS

The effects of CWT and CWHF boundary conditions on laminar natural convection of yield stress fluid following the Bingham model in square enclosures with differentially heated horizontal walls have been analyzed numerically in this analysis for a range of different values of nominal Rayleigh (ranging from 10^3 to 10^5) and Prandtl (ranging from 0.1 to 100) numbers. It has been found that the mean Nusselt number $\overline{\text{Nu}}$ increases with increasing Rayleigh number but $\overline{\text{Nu}}$ is found to be smaller in Bingham fluids than in Newtonian fluids for the same nominal values of Rayleigh and Prandtl numbers due to stronger flow resistance in Bingham fluids. Moreover, $\overline{\text{Nu}}$ monotonically decreases with increasing Bingham number irrespective of the boundary condition. Bingham fluids are shown to exhibit a nonmonotonic Pr dependence on $\overline{\text{Nu}}$ and a detailed physical explanation has been provided for this behavior. Although variation of $\overline{\text{Nu}}$ in response to changes in Rayleigh, Prandtl, and Bingham numbers remains qualitatively similar for both CWT and CWHF boundary conditions, $\overline{\text{Nu}}$ for the CWHF boundary condition assumes smaller values than in the CWT configuration for large values of Rayleigh number for a given set of values of Prandtl and Bingham numbers. Detailed scaling analysis has been carried out to explain the differences in the heat transfer behavior between the CWT and CWHF boundary conditions. Guided by this scaling analysis, correlations of the mean Nusselt number $\overline{\text{Nu}}$ have been proposed for natural convection of Bingham fluids in square enclosures with differentially heated horizontal walls for both CWT and CWHF boundary conditions. It has been shown that the proposed correlations satisfactorily capture the variation of $\overline{\text{Nu}}$ in response to the changes in Rayleigh, Prandtl, and Bingham numbers for the cases considered here. It is worth noting that thermal conductivity, specific heat, plastic viscosity, and yield stress are considered to be independent of temperature in this analysis and the effects of the aforementioned temperature dependence will be investigated in future analyses by the present authors.

REFERENCES

Balmforth, N. J. and Rust, A. C., Weakly nonlinear viscoplastic convection, *J. Non-Newtonian Fluid Mech.*, vol. **158**, pp. 36–45, 2009.

Barnes, H. A., The yield stress—a review or '$\pi\alpha\nu\tau\alpha\ \rho\epsilon\iota$'—everything flows?, *J. Non-Newtonian Fluid Mech.*, vol. **81**, pp. 133–178, 1999.

Bejan, A., *Convection Heat Transfer*, New York: John Wiley Sons, Inc., 1984.

Beverly, C. R. and Tanner, R. I., Numerical analysis of extrudate swell in viscoelastic materials with yield stress, *J. Rheol.*, vol. **33**, no. 6, pp. 989–1006, 1989.

Corcione, M., Effects of the thermal boundary conditions at the sidewalls upon natural convection in rectangular enclosures heated from below and cooled from above, *Int. J. Therm. Sci.*, vol. **42**, pp. 199–208, 2003.

de Vahl Davis, G., Natural convection of air in a square cavity: A bench mark numerical solution, *Int. J. Numer. Meth. Fluids*, vol. **3**, pp. 249–264, 1983.

Gebhart, B., Effects of viscous dissipation in natural convection, *J. Fluid Mech.*, vol. **14**, pp. 225–232, 1962.

Lamsaadi, M., Nami, M., Hasnaoui, M., and Mamou, M., Natural convection in a vertical rectangular cavity filled with a non-Newtonian power law fluid and subjected to a horizontal temperature gradient, *Numer. Heat Transfer, Part A*, vol. **49**, pp. 969–990, 2006.

Mitsoulis, M., Flows of viscoplastic materials: Models and computations, in *Rheology Reviews*, edited by Binding, D. M., Hudson, N. E., and Keunings, R.,British Society of Rheology, London, UK, pp. 135–178, 2007.

Mitsoulis, E. and Zisis, T., Flow of Bingham plastics in a lid-driven square cavity, *J. Non-Newtonian Fluid Mech.*, vol. **101**, pp. 173–180, 2001.

O'Donovan, E. J. and Tanner, R. I., Numerical study of the Bingham squeeze film problem, *J. Non-Newtonian Fluid Mech.*, vol. **15**, pp. 75–83, 1984.

Ostrach, S., Natural convection in enclosure, *J. Heat Transfer*, vol. **110**, pp. 1175–1190, 1988.

Ozoe, H. and Churchill, S. W., Hydrodynamic stability and natural convection in Ostwald–De Waele and Ellis fluids: the development of a numerical solution, *AIChE J.*, vol. **18**, pp. 1196–1207, 1972.

Park, H. M. and Ryu, D. H., Rayleigh–Bénard convection of viscoelastic fluids in finite domains, *J. Non-Newtonian Fluid Mech.*, vol. **98**, pp. 169–184, 2001.

Patankar, S. V., *Numerical Heat Transfer and Fluid Flow*, Washington, D.C.: Hemisphere, 1980.

Papanastasiou, T. C., Flow of materials with yield, *J. Rheol.*, vol. **31**, pp. 385–404, 1987.

Peixinho, J., Desaubry, C., and Lebouche, M., Heat transfer of a non-Newtonian fluid (Carbopol aqueous solution) in transitional pipe flow, *Int. J. Heat Mass Transfer*, vol. **51**, pp. 198–209, 2008.

Quertatani, N., Cheikh, N. B., Beya, B. B., and Lili, T., Numerical simulation of two dimensional Rayleigh–Bénard convection in an enclosure, *C. R. Mecanique*, vol. **336**, pp. 464–470, 2008.

Roache, P. J., Quantification of uncertainty in computational fluid dynamics, *Annu. Rev. Fluid Mech.*, vol. **29**, pp. 123–160, 1997.

Turan, O., Chakraborty, N., and Poole, R. J., Laminar natural convection of Bingham fluids in a square enclosure with differentially heated side walls, *J. Non-Newtonian Fluid Mech.*, vol. **165**, pp. 901–913, 2010.

Turan, O., Sachdeva, A., Poole, R. J., and Chakraborty, N., Laminar natural convection of Bingham fluids in a square enclosure with vertical walls subjected to constant heat flux, *Numer. Heat Transfer A*, vol. **60**, pp. 381–409, 2011.

Vikhansky, A., Thermal convection of a viscoplastic liquid with high Rayleigh and Bingham numbers, *Phys. Fluids*, vol. **21**, pp. 103103, 2009.

Vikhansky, A., On the onset of Bingham liquid in rectangular enclosures, *J. Non-Newtonian Fluid Mech.*, vol. **165**, pp. 901–913, 2010.

Vola, D., Boscardin, L., and Latché, J. C., Laminar unsteady flows of Bingham fluids: A numerical strategy and some benchmark results, *J. Comput. Phys.*, vol. **187**, pp. 441–456, 2003.

Zhang, J., Vola, D., and Frigaard, I. A., Yield stress effects on Rayleigh–Bénard convection, *J. Fluid Mech.*, vol. **566**, pp. 389–419, 2006.